

# Light baryon spectra and Regge trajectories from anomalous holographic hard wall models

Rafael A. Costa-Silva\* and Henrique Boschi-Filho†

*Instituto de Física, Universidade Federal do Rio de Janeiro,*

*21.941-909, Rio de Janeiro, RJ, Brazil*

(Dated: March 18, 2026)

## Abstract

In this work we propose anomalous versions of the holographic hard wall (HW) model to describe the spectra of light baryons of spin  $1/2$  and  $3/2$ , and obtain their Regge trajectories. The anomalous contributions to the dimensions of the baryonic operators of logarithm form come from a semiclassical analysis of the AdS/CFT correspondence and were used recently for glueballs and light unflavoured mesons. Inspired by these results, we first propose an anomalous dimension of the form  $\Delta_{\text{anom.}} = a \ln L + b$ , where  $a$  and  $b$  are phenomenological constants to be adjusted numerically to better fit the experimental data of the PDG, and  $L$  is the angular momentum of each baryonic state. Second, we discuss the case where the anomalous dimension also depends on the spin  $S$  as  $\Delta_{\text{anom.}} = a \ln(L + S + 1/2) + b$ , and fix the parameters  $a$  and  $b$  targeting PDG data. These two models, called  $\text{AHW}_1$  and  $\text{AHW}_2$ , give better results for light baryon masses ( $M$ ) in comparison with the original HW model and show approximately linear Regge trajectories ( $M^2 \times L$ ). We also consider a third anomalous HW model in which the dimension of the baryonic operator increases as  $\Delta_{\text{Lin.}} = aL^c + b$ , where  $a$ ,  $b$ , and  $c$  are constants adjusted to fit the light baryonic masses of PDG. Apart from compatible masses with PDG data, this case produces Regge trajectories that are asymptotically linear.

---

\* rafaelfcosta@pos.if.ufrj.br; rc-fis@outlook.com

† boschi@if.ufrj.br; hboschi@gmail.com

## I. INTRODUCTION

Understanding the nonperturbative regime of Quantum Chromodynamics (QCD) remains one of the main open problems in strong interaction physics. Although perturbative techniques successfully describe high-energy processes, the low-energy sector — where confinement and bound states emerge — still requires effective approaches. In particular, the structure of the baryon spectrum and the approximate linear behavior of Regge trajectories provide important phenomenological constraints that any realistic model should reproduce (see, *e.g.*, [1, 2]).

The gauge/gravity correspondence, originally formulated in the context of the AdS/CFT correspondence [3–6], offers a powerful framework to investigate strongly coupled gauge theories through dual gravitational descriptions. Although QCD is neither supersymmetric nor conformal, bottom-up holographic constructions have proven useful in incorporating essential features of low-energy hadron physics in an effective manner (see, *e.g.* [7, 8]).

Among these constructions, the hard wall (HW) model [9–12] introduces an infrared cutoff in AdS space to mimic confinement, generating discrete mass spectra for hadronic states. This framework has been successfully applied to glueballs, mesons, and baryons [11–15]. Despite these successes, some limitations are well known. In particular, the original Hard Wall setup does not naturally produce asymptotically linear Regge trajectories, and the degeneracy patterns depend sensitively on the choice of scaling dimensions assigned to the boundary operators. Linear Regge trajectories were obtained soon after with the soft wall model [16, 17].

The hard and soft wall models were applied to a variety of problems, from spectra and Regge trajectories [18–27], the determination of form factors, decay constants and couplings [28–37], high energy scattering [38–55], the holographic construction of the Cornell potential [56–59], dynamical corrections to the soft wall model [60–67], finite temperature and density effects and the confinement-deconfinement phase transition [68–91], magnetic susceptibility, magnetic and inverse magnetic catalysis [92–99], entanglement [100, 101], weak-interacting holographic QCD [102], technicolor modeling [103–105], the muon  $g - 2$  problem [106–110], gluon and pion condensates [111–113],  $1/N_c$  corrections and large  $N$  effects [114, 115], nuclei properties [116–120], and to fluids and condensed matter systems [121–127].

Despite these many successes, the non-linearity of the Regge trajectories obtainable from

the hard wall model persists. This situation changed by considering anomalous dimensions for the hadronic operators in the case of glueballs [128] and light unflavoured mesons [129].

Experimental data compiled by the Particle Data Group (PDG) [130] show a rich structure for nucleon and delta resonances, including approximate linear Regge behavior and systematic organization of parity. Reproducing these features within a holographic framework requires a careful treatment of the relation between bulk fermion masses and the scaling dimensions of the corresponding boundary operators. In interacting quantum field theories, operator dimensions generally receive anomalous contributions due to renormalization effects (see, *e.g.* [1, 2]).

Motivated by semiclassical analyses of large-spin operators in the gauge/gravity correspondence [131] and by previous successful applications of anomalous dimensions in holographic models for glueballs and light mesons [128, 129], we investigate the impact of including anomalous contributions in the baryonic hard wall framework.

In this work, we first revisit the description of fermionic fields in  $\text{AdS}_5$ , deriving the equations of motion for the spin-1/2 and spin-3/2 fields and reviewing the relation between the bulk mass parameters and the operator dimensions. We reconstruct the baryon spectrum in the original Hard Wall model, allowing for distinct canonical dimensions for different spins. We then introduce logarithmic realizations of anomalous dimensions and analyze their phenomenological consequences through a numerical minimization procedure based on experimental data. In addition, we explore a linear variant of the anomalous dimension aimed at improving the asymptotic behavior of Regge trajectories.

Our main objective is to assess whether the inclusion of anomalous dimensions within the Hard Wall approach can provide a more realistic description of light baryon spectra while preserving the simplicity of the bottom-up holographic construction.

The paper is organized as follows. In Section II we review fermions in AdS space. Section III presents the experimental input and statistical definitions. In Section IV we discuss the original and anomalous HW models. The numerical results are discussed in Section V, followed by an anomalous linear hard wall model in Section VI, and we conclude in Section VII with a discussion of the results and possible future developments.

$L$	$S$	Nucleon Resonances
0	1/2	$N_{1/2+}(939)$
1	1/2	$N_{1/2-}(1535), N_{3/2-}(1520)$
1	3/2	$N_{1/2-}(1650), N_{3/2-}(1700), N_{5/2-}(1675)$
2	1/2	$N_{3/2+}(1720), N_{5/2+}(1680)$
2	3/2	$N_{1/2+}(1880), N_{3/2+}(1900), N_{5/2+}(1870), N_{7/2+}(1990)$
3	1/2	$N_{5/2-}(2200), N_{7/2-}(2190)$
3	3/2	$N_{9/2-}(2250)$
4	1/2	$N_{9/2+}(2220)$
5	1/2	$N_{11/2-}(2600)$
6	1/2	$N_{13/2+}(2700)$

TABLE I. Nucleon resonances states  $N_{J,P}(M)$  with masses  $M$  in MeV from PDG.

$L$	$S$	Delta Resonances
0	3/2	$\Delta_{3/2+}(1232)$
1	1/2	$\Delta_{1/2-}(1620), \Delta_{3/2-}(1700)$
2	3/2	$\Delta_{1/2+}(1910), \Delta_{3/2+}(1920), \Delta_{5/2+}(1905), \Delta_{7/2+}(1950)$
3	1/2	$\Delta_{7/2-}(2200)$
4	3/2	$\Delta_{7/2+}(2390), \Delta_{9/2+}(2300), \Delta_{11/2+}(2420)$
6	3/2	$\Delta_{15/2+}(2950)$

TABLE II. Delta resonances states  $\Delta_{J,P}(M)$  with masses  $M$  in MeV from PDG.

## II. PDG DATA AND STATISTICAL DEFINITIONS

In this section, we present the masses for the PDG nucleon and delta resonances [130] and the statistical functions used to perform the numerical analysis. The resonances are separated into their respective families for each fixed  $L$  and  $S$ , where these correspond, respectively, to the orbital angular momentum and the intrinsic spin, in Tables I and II. Note that these states are also classified by their parity  $P$ , which is determined by their angular momentum states:  $L$  even (odd) corresponds to positive (negative) parity.

In particular, we begin by presenting the functions that we use to determine the best fit of PDG masses from the proposed HW models. We first define the deviation between our estimated  $m_i$  and the PDG  $M_i$  masses

$$\delta_i = \frac{|M_i - m_i|}{M_i}. \quad (1)$$

In addition, we define the function  $Q$ ,

$$Q = \sqrt{\sum_i \delta_i^2}, \quad (2)$$

which will be minimized to determine the best fit of our models compared to PDG data.

### III. BRIEF REVIEW OF FERMIONS IN ADS SPACE

Here, in this section, we briefly review the basic properties of the AdS space and how to describe fermionic fields with spins 1/2 and 3/2 in its bulk. The AdS<sub>5</sub> space can be conveniently defined by the Poincaré patch with metric [6]

$$ds^2 = g_{MN}dx^M dx^N = \frac{R^2}{z^2} (\eta^{\mu\nu} dx_\mu^2 dx_\nu^2 + dz^2), \quad (3)$$

where  $\eta_{\mu\nu} = \text{diag}(-1, 1, 1, 1)$  is the flat four-dimensional Minkowski metric with  $\mu, \nu = 0, 1, 2, 3$  while  $M, N = 0, 1, 2, 3, 5$  tags the five-dimensional AdS<sub>5</sub> space. The holographic coordinate  $z$  is defined in the interval  $[0, \infty)$ , and  $z = 0$  corresponds to a boundary of the AdS space. The fields defined in the bulk of the AdS<sub>5</sub> space typically span over the five coordinates  $x^M$ .

#### A. Fermions with spin 1/2

The Dirac equation in the 4-dimensional Minkowski space is

$$(\gamma^\mu \partial_\mu - m)\psi(x) = 0, \quad (4)$$

with,

$$\{\gamma^\mu, \gamma^\nu\} = 2\eta^{\mu\nu}. \quad (5)$$

Defining the Dirac equation in a 5-dimensional flat spacetime requires five gamma matrices that satisfy an extension of the relation (5). A natural choice is obtained by making

[132, 133]

$$\Gamma_\mu = \gamma_\mu \quad ; \quad \Gamma_5 = \gamma_5, \quad (6)$$

where  $\gamma_5 = -i\gamma^0\gamma^1\gamma^2\gamma^3$ . The matrices defined in this way satisfy the relation

$$\{\Gamma_M, \Gamma_N\} = 2\eta_{MN}. \quad (7)$$

If we want to obtain the Dirac equation in AdS<sub>5</sub>, we need to use vielbein. Locally the curved spacetime at a point P can have the metric tensor given by the Minkowski metric in a special coordinate system. Let  $\xi^\alpha$  be the coordinates of this point in this frame. The vielbein is a set of vectors given by

$$e_\mu^\alpha = \partial_\mu \xi^\alpha, \quad (8)$$

where  $x$ , present in the derivative, are the coordinates of P in the general frame with metric  $g_{\mu\nu}(x)$ . The following relation holds:

$$\eta_{\alpha\beta} e_\mu^\alpha e_\nu^\beta = g_{\mu\nu}. \quad (9)$$

Generally, if we define

$$\tilde{\Gamma}_M = e_M^N \Gamma_N, \quad (10)$$

we can see that an analogous relation to that satisfied in flat space is obtained, given by

$$\{\tilde{\Gamma}_M, \tilde{\Gamma}_N\} = 2g_{MN} \quad (11)$$

In particular, for AdS<sub>5</sub>, the inertial coordinates are  $\xi^A = \frac{1}{z}x^A$ , so the vielbein reads

$$e_N^M = \frac{R}{z} \delta_N^M. \quad (12)$$

In order to write the Dirac equation in a curved spacetime, we need to replace the partial derivative in (4) by a covariant derivative. The covariant derivative of a spinor is given by

$$D_M = \partial_M + \frac{1}{4} \omega_M^{AB} \Sigma_{AB}, \quad (13)$$

where  $\Sigma_{AB} = \frac{1}{2}[\Gamma_A, \Gamma_B]$  is the generator for Lorentz transformations of a spinor. The  $\omega_M^{AB}$  is the spin connection and indicates the behaviour of the vielbein if transported.

$$\omega_M^{AB} = \frac{1}{2} \left( e_N^A \partial_M g^{NP} e_P^B + e_N^A g^{QR} e_R^B \Gamma_{QM}^N - (A \leftrightarrow B) \right). \quad (14)$$

The only non-vanishing Christoffel symbols are

$$\Gamma_5^{55} = A'(z) \quad ; \quad \Gamma_{MN}^5 = -A'(z)\eta_{MN} \quad ; \quad \Gamma_{5N}^M = A'(z)\delta_N^M. \quad (15)$$

So, the non-vanishing spin connection is

$$\omega_M^{5A} = -\omega_M^{A5} = -A'(z)\delta_M^A. \quad (16)$$

Substituting these results in (13), we obtain

$$D_5 = \partial_5 \quad ; \quad D_\mu = \partial_\mu - \frac{1}{2z}\Gamma_\mu\Gamma_5. \quad (17)$$

Finally, in analogy with (4), we write the Dirac equation in AdS<sub>5</sub>

$$(\tilde{\Gamma}^M D_M - m_5)\psi(x, z) = \left( \gamma^\mu \partial_\mu - \frac{2}{z}\gamma_5 + \gamma_5 \partial_z - \frac{m_5 R}{z} \right) \psi(x, z) = 0. \quad (18)$$

Now, we make an *ansatz* of plane wave solution

$$\psi(x, z) = e^{-ip \cdot x} u(p) \phi(z), \quad (19)$$

where the Dirac spinors follow

$$\gamma^\mu \partial_\mu [e^{-ip \cdot x} u(p)] = M [e^{-ip \cdot x} u(p)], \quad (20)$$

with  $M$  the mass of the fermions in the 4-dimensional flat boundary. Let us split the solutions by chirality in left and right (+/-) modes,

$$\psi_\pm = e^{-ip \cdot x} u_\pm(p) \phi_\pm(z). \quad (21)$$

By definition, we have that  $\gamma_5 u_\pm = \pm u_\pm$  and the following relation holds:

$$\gamma^\mu \partial_\mu (e^{-ip \cdot x} u_\pm) = M (e^{-ip \cdot x} u_\mp). \quad (22)$$

Back with these definitions and relations in (18), we find

$$\left( \gamma^\mu \partial_\mu - \frac{m_5 R}{z} \right) (\psi_+ + \psi_-) + \left( \gamma_5 \partial_z - \frac{2}{z}\gamma_5 \right) (\psi_+ + \psi_-) = 0, \quad (23)$$

so,

$$M \left( \phi_+ u_- + \phi_- u_+ \right) - \frac{m_5 R}{z} \left( \phi_+ u_+ + \phi_- u_- \right) + \left( \partial_z - \frac{2}{z} \right) \left( \phi_+ u_+ - \phi_- u_- \right) = 0. \quad (24)$$

Comparing the terms with chirality left, we find

$$\left(\partial_z - \frac{2 + m_5 R}{z}\right)\phi_+ = -M\phi_-. \quad (25)$$

Similarly, the right spinors give us

$$\left(\partial_z - \frac{2 - m_5 R}{z}\right)\phi_- = M\phi_+. \quad (26)$$

The equations (25) and (26) can be used together to write two equations of second order,

$$\left[\partial_z^2 - \frac{2}{z} + \frac{5^2 - 4(m_5 R \mp 1/2)^2}{4z^2} + M^2\right]\phi_{\pm}(z) = 0. \quad (27)$$

Defining  $\nu_{\pm} = (m_5 R \mp 1/2)$ , and making the substitution  $\phi_{\pm}(z) = z^{5/2}f_{\pm}(z)$ , the equations become

$$z^{5/2}[z^2\partial_z^2 + z\partial_z + (M^2z^2 - \nu_{\pm}^2)]f_{\pm}(z) = 0. \quad (28)$$

These equations for  $f_{\pm}(z)$  are the Bessel equations whose solutions are linear combinations of the Bessel and Neumann functions of order  $\nu_{\pm}$ . We are interested in regular solutions at  $z = 0$ , so we take the coefficients related to Neumann solutions as zero for all modes; in this way, the solutions are

$$\phi_{\pm}(z) = C_{\pm}z^{5/2}J_{\nu_{\pm}}(z). \quad (29)$$

For fermions, the connections between the scaling dimension and the mass in the bulk are given by

$$\Delta = 2 + |m_5 R|, \quad (30)$$

and baryons with spin  $S = 1/2$  in four dimensions, the mass dimension is

$$\Delta = \frac{9}{2} + L. \quad (31)$$

Combining Eqs. (30) and (31), one finds  $|m_5 R| = L + 5/2$ , which substituted in Eq. (27) gives  $\nu_- = \alpha + 1$  and  $\nu_+ = \alpha$ , where we defined  $\alpha = 2 + L$ . With these definitions, we find the full plane wave solution in terms of right and left chirality

$$\psi_{\alpha}(x, z) = e^{-ip \cdot x} z^{5/2} [C_{\alpha} J_{\alpha}(m_{\alpha} z) u_+(p) + C_{\alpha+1} J_{\alpha+1}(m_{\alpha+1} z) u_-(p)], \quad (32)$$

where the parameters  $m_{\alpha}$  and  $m_{\alpha+1}$  have dimension of mass, such that the arguments of the Bessel functions are dimensionless.

Before we proceed implementing the phenomenological model and comparing to experimental data, let us discuss higher half-integer spin fields.

## B. Fermions with spin 3/2

Fermions with higher spins can be described by objects that mix spinor and tensor indices [134],  $\psi_{\beta, \{\mu_1 \dots \mu_n\}}$ , where  $\beta$  is the spinor index;  $\mu_i$  are vector indices, and  $\{\dots\}$  means symmetrization of the indices. To describe fermions with spin 3/2, we have the Rarita-Schwinger equation. In the original paper, their expression suggests an alternative form given by

$$(\gamma^{[\mu} \gamma^{\nu} \gamma^{\lambda]} \partial_{\nu} + m \gamma^{[\mu} \gamma^{\lambda]}) \psi_{\lambda} = 0, \quad (33)$$

where  $[\dots]$  means anti-symmetrization of the indices. This form can be extended to non-Euclidean geometry

$$(\tilde{\Gamma}^{[M} \tilde{\Gamma}^N \tilde{\Gamma}^L] \partial_N + m \tilde{\Gamma}^{[M} \tilde{\Gamma}^L]) \psi_L = 0. \quad (34)$$

Introducing

$$\hat{\psi}_A = e_A^M \Psi_M, \quad (35)$$

and choosing  $\Psi_5 = 0$  it has been shown [134] that  $\hat{\psi}_A$  satisfies indeed an equation of the form (18). It is

$$(\gamma^{\nu} \partial_{\nu} - m) \psi_{\{\mu_1 \dots \mu_n\}} = 0 \quad ; \quad \gamma^{\mu_1} \psi_{\{\mu_1 \dots \mu_n\}} = 0. \quad (36)$$

Indeed, the general solution can be obtained from the Dirac equation with covariant derivative, but all tensor indices referring to the inertial frame, so we introduce

$$\hat{\psi}_{\{A_1 \dots A_n\}} = e_{A_1}^{M_1} \dots e_{A_n}^{M_n} \psi_{\{A_1 \dots A_n\}}, \quad (37)$$

which satisfy the Dirac equation (18)

$$(\tilde{\Gamma}^M D_M - m) \hat{\psi}_{\{A_1 \dots A_n\}} = 0. \quad (38)$$

In anti-de Sitter space, we have  $\hat{\psi}_{\{A_1 \dots A_n\}} = z^n \psi_{\{A_1 \dots A_n\}}$ . In particular, for spin 3/2 we have  $\hat{\psi}_{\mu} = z \psi_{\mu}$ , substituting this relation in (18), we obtain equations similar to the spin 1/2 case. The second order equations become

$$\left[ \partial_z^2 - \frac{3}{z} + \frac{7^2 - 4(m_5 R \mp 1/2)^2}{4z^2} + M^2 \right] \phi_{\pm}(z) = 0, \quad (39)$$

and the solutions can be written as

$$z^{7/2} [z^2 \partial_z^2 + z \partial_z + (M^2 z^2 - \nu_{\pm}^2)] f_{\pm}(z) = 0. \quad (40)$$

Here, since we are considering a spin  $S = 3/2$  particle as a sum of a spin  $S = 1$  and another  $S = 1/2$ , we will interpret such fields as a vector field and a spin-1/2 field, which leads us to the dimension

$$\Delta = \frac{11}{2} + L, \quad (41)$$

whose solutions will be

$$\psi_\alpha^\mu(x, z) = \epsilon^\mu e^{-ip \cdot x} z^{7/2} [C_{\alpha+1} J_{\alpha+1}(m_{\alpha+1} z) u_+(p) + C_{\alpha+2} J_{\alpha+2}(m_{\alpha+2} z) u_-(p)], \quad (42)$$

where  $\alpha = 2 + L$ , as in the case of spin 1/2 fermions. Note that here the positive parity index for the Bessel functions is  $\nu_+ = \alpha + 1$ , while for the negative parity it is  $\nu_- = \alpha + 2$ . With these solutions, we can construct the HW mass tower.

#### IV. A HARD WALL MODEL AND ANOMALOUS VERSIONS

In this section, we discuss the holographic Hard Wall model (HW), based on the idea previously developed in [11–15] and propose an improved version of the Anomalous Hard Wall model (AHW) for baryons, previously developed for glueballs and light mesons [128, 129]. Unlike the original HW model for baryons [13], this version differs since we assign distinct mass dimensions to spin-1/2 and spin-3/2 objects.

The main idea of the hard wall model is to introduce a hard cut off in the AdS space breaking conformal invariance. This was proposed by Polchinski and Strassler to study the hard scattering of glueballs [9] and was adopted to calculate scalar glueball masses in Refs. [11, 12]. In Poincaré coordinates, Eq. (3), one can set

$$\frac{1}{z_{\max}} = \Lambda_{\text{HW}}, \quad (43)$$

where in this model, the holographic coordinate  $z$  is now defined in the range  $[0, z_{\max}]$ . This sets a mass/energy scale for the hard wall model. Then, a boundary condition is imposed in  $z = z_{\max}$  discretizing the field wave functions implying discrete mass spectra, and the mass parameters  $m_\alpha$  become related to the  $k$ -th zeros  $\chi_{\alpha,k}$  of a given Bessel function  $J_\alpha(m_{\alpha,k} z)$ . This model was later extended to mesons and baryons [13, 14] and higher spin glueballs [15]. Since in this work we are not considering radial excitations, the masses of the baryons will all have fixed  $k = 1$ , which we are going to omit from now on.

### A. Hard Wall Model

As discussed in Section III, fermionic solutions with spin 1/2 and 3/2, Eqs. (32) and (42), are described by two modes, each with positive and negative parities. In order to obtain the masses associated with each of the modes, we now impose boundary conditions at  $z = z_{\max}$  on these solutions; in particular, we impose Dirichlet boundary conditions. Clearly, we cannot simultaneously impose such conditions on both modes, so each mode has its own spectrum. As in [13], the right-handed mode will be associated with the positive-parity spectrum, while the left-handed mode will correspond to the negative-parity spectrum. The parity  $P$  of the states is connected to their orbital angular momentum  $L$ . Particles with even (odd)  $L$  have positive (negative) parity.

Thus, for the spin-1/2 we have from Eq. (32) and setting the positive parity so that  $\nu = \nu_+ = \alpha = 2 + L$  we obtain,

$$M_{1/2+}(L) = \chi_{2+L}\Lambda_{\text{HW}}; \quad (\text{nucleons}). \quad (44)$$

This equation applies for nucleons since these particles have spin 1/2 states with positive parity, which is not the case for deltas, as can be seen from PDG data compiled in Tables I and II.

For spin-1/2 and negative parity, we have from Eq. (32) and  $\nu = \nu_- = \alpha + 1 = 3 + L$ , so that

$$M_{1/2-}(L) = \chi_{3+L}\Lambda_{\text{HW}}; \quad (\text{nucleons and deltas}). \quad (45)$$

Note that this equation applies equally well for nucleons and deltas since both particles have states with spin 1/2 and negative parity, as can be checked in Tables I and II.

For spin-3/2 the solution comes from the Rarita-Schwinger equation, Eq. (42). Then, choosing the positive parity solution  $u_+$ , we have  $\nu = \nu_+ = \alpha + 1 = 3 + L$ , so that

$$M_{3/2+}(L) = \chi_{3+L}\Lambda_{\text{HW}}; \quad (\text{nucleons and deltas}), \quad (46)$$

which applies to nucleons and deltas, according to PDG data, Tables I and II.

For spin-3/2 and negative parity, one still resourses to Eq. (42) with  $\nu = \nu_- = \alpha + 2 = 4 + L$ , then

$$M_{3/2-}(L) = \chi_{4+L}\Lambda_{\text{HW}}; \quad (\text{nucleons}), \quad (47)$$

which applies only to nucleons, once deltas do not have spin 3/2 with negative parity.

Note also that the masses for negative parity with spin 1/2, Eq. (45) and positive parity with spin 3/2, Eq. (46), coincide, both for nucleons and deltas, so these states and the corresponding Regge trajectories will be degenerate.

The mass scale  $\Lambda_{\text{HW}}$  is chosen to obtain the best fit of the masses tabulated by PDG. Then, we look for the value that minimizes the function  $Q$ , defined in equation (2). This is done separately for nucleons and deltas implying two values of  $\Lambda_{\text{HW}}$ , one for each family. We will solve this problem numerically in Section IV C. The results are shown in Tables IV and V. The corresponding Regge trajectories obtained from this version of the hard wall model are shown in Fig. 1.

## B. Anomalous Hard Wall Models

Now, we proceed to discuss the anomalous hard wall model for baryons. It is a well known fact that in an interacting field theory, the anomalous dimension plays an important role due to renormalization. Since baryons are made of interacting three valence quarks, it is reasonable that the mass dimension of an operator that corresponds to a baryon state is not simply the sum over canonical dimensions (free theory) of such quarks but is corrected by the anomalous dimension. In order to treat the dimension of such operators we will write the total dimension,  $\Delta$  as a sum of the canonical part (no interacting theory) and the anomalous one. So, we consider that the total dimension of a hadronic operator ( $\Delta_{\text{total}}$ ) is the sum of its canonical dimension ( $\Delta_{\text{can.}}$ ) plus its anomalous dimensions ( $\Delta_{\text{anom.}}$ ):

$$\Delta_{\text{total}} = \Delta_{\text{can.}} + \Delta_{\text{anom.}}. \quad (48)$$

The canonical dimension  $\Delta_{\text{can.}}$  was discussed in Sect. III for spins 1/2 and 3/2, in Eqs. (31) and (41), respectively,

$$\Delta_{\text{can.}} = \begin{cases} \frac{9}{2} + L; & S = 1/2, \\ \frac{11}{2} + L; & S = 3/2. \end{cases} \quad (49)$$

It is important to note that both nucleons and deltas can have spin-1/2 or spin-3/2. Therefore, whether the canonical dimension will be given by the first or second of the equations (49) will depend only on its spin and not on the family of the particle.

From a semiclassical gauge/gravity duality [131], the anomalous dimension of an operator at the boundary increases logarithmically with its total angular momentum  $J$

$$\Delta_{\text{anomalous}} = \frac{\sqrt{\lambda}}{\pi} \ln \left( \frac{J}{\sqrt{\lambda}} \right) + \mathcal{O}(J^0), \quad (50)$$

where  $\lambda = g_{\text{YM}}^2 N$  is the 't Hooft coupling for an  $SU(N)$  Yang-Mills theory. The above relation is valid when  $\lambda \gg 1$ .

Inspired by this result, we will propose anomalous corrections to the hard wall model. First, we suppose that the anomalous dimension depends only on the orbital angular momentum excitation  $L$ , and is given by

$$\Delta_{\text{anom.1}} = a \ln(L + 1) + b, \quad (51)$$

where  $a$  and  $b$  are free parameters to be adjusted to fit PDG data. Note that we have chosen the argument of the logarithm as  $L + 1$  in order to avoid a singularity in the the ground state  $L = 0$ .

In our second proposal, the anomalous dimension depends on  $L$ , the orbital angular momentum excitation, and  $S$ , the intrinsic spin. To make (for  $S = 1/2$ ) the anomalous dimension related to the first case, we write

$$\Delta_{\text{anom.2}} = a \ln(L + S + 1/2) + b, \quad (52)$$

where  $a$  and  $b$  are again free parameters that will be fixed later.

So, one can go back to the discussion of Section III and substitute the canonical dimensions for spins  $1/2$  and  $3/2$ , Eqs. (31) and (41), respectively, by the total dimension given by Eq. (48), with the anomalous dimensions given by (51) or (52), which we call, respectively, AHW1 and AHW2. This implies that we replace  $\alpha = 2 + L$  by  $\alpha = 2 + L + \Delta_{\text{anom.1}}$  or by  $\alpha = 2 + L + \Delta_{\text{anom.2}}$ .

The energy scale parameter, previously denoted by  $\Lambda_{\text{HW}}$ , which here will be denoted as  $\Lambda_{\text{AHW}}$ , is obtained as before: minimizing the function in (2); for simplicity, we will make this parameter the same for the two versions of the anomalous dimension analyzed.

The masses of the positive-parity spin states  $1/2$  from Eq. (32) and  $\nu = \nu_+ = \alpha = 2 + L + \Delta_{\text{anom.}}$  we obtain for nucleons

$$M_{1/2+}(L) = \chi_{2+L+\Delta_{\text{anom.}}} \Lambda_{\text{AHW}}; \quad (\text{nucleons}), \quad (53)$$

and for spin 1/2 and negative parity with  $\nu = \nu_- = \alpha + 1 = 3 + L + \Delta_{\text{anom.}}$ , one has for nucleons and deltas

$$M_{1/2-}(L) = \chi_{3+L+\Delta_{\text{anom.}}}\Lambda_{\text{AHW}}; \quad (\text{nucleons and deltas}). \quad (54)$$

For spin-3/2, with solution given by Eq. (42), and positive parity, we have  $\nu = \nu_+ = \alpha + 1 = 3 + L + \Delta_{\text{anom.}}$  for nucleons and deltas

$$M_{3/2+}(L) = \chi_{3+L+\Delta_{\text{anom.}}}\Lambda_{\text{AHW}}; \quad (\text{nucleons and deltas}), \quad (55)$$

and for spin 3/2 and negative parity,  $\nu = \nu_- = \alpha + 2 = 4 + L + \Delta_{\text{anom.}}$  for nucleons

$$M_{3/2-}(L) = \chi_{4+L+\Delta_{\text{anom.}}}\Lambda_{\text{AHW}}; \quad (\text{nucleons}). \quad (56)$$

Note that the masses for negative parity with spin 1/2, Eq. (54) and positive parity with spin 3/2, Eq. (55), do coincide for  $\Delta_{\text{anom.}1}$ , Eq. (51), as in the case of the usual hard wall model, for nucleons and deltas, but not for  $\Delta_{\text{anom.}2}$ , Eq. (52), as can be seen in Figs. 2 and 3.

The parameters  $\Lambda_{\text{AHW}}$  in the above equations and  $a$ , and  $b$  in Eqs. (51) and (52), are obtained by minimizing the function  $Q$ , Eq. (2), which we solve numerically in the next section, showing the results of both possibilities for the proposed anomalous dimensions. The corresponding masses are shown in Tables IV and V, and the Regge trajectories in Figs. 2 and 3.

### C. Numerical Results for the HW and AHW models

In this section, we present the numerical results for the Hard Wall and Anomalous Hard Wall models proposed in previous sections and compare them with PDG data. In order to obtain the mass values from these models given a state with orbital angular momentum  $L$  and spin  $S$ , we need to use the appropriate equation from (44)-(47), in the HW case, or from (53)-(56) for the AHW. As mentioned above, the parameters  $a$ ,  $b$  and the energy scale  $\Lambda$  are obtained by minimizing the function  $Q$  in equation (2). Since this function depends on the obtained masses, it is a recursive problem that we solve numerically and present the values of the parameters, as well as the masses for each state and each model.

In Table III, we present the numerical values for  $\Lambda$ , the energy scale, the values of the parameters  $a$  and  $b$ , and the values of the function  $Q$  divided by the number  $n$  of states

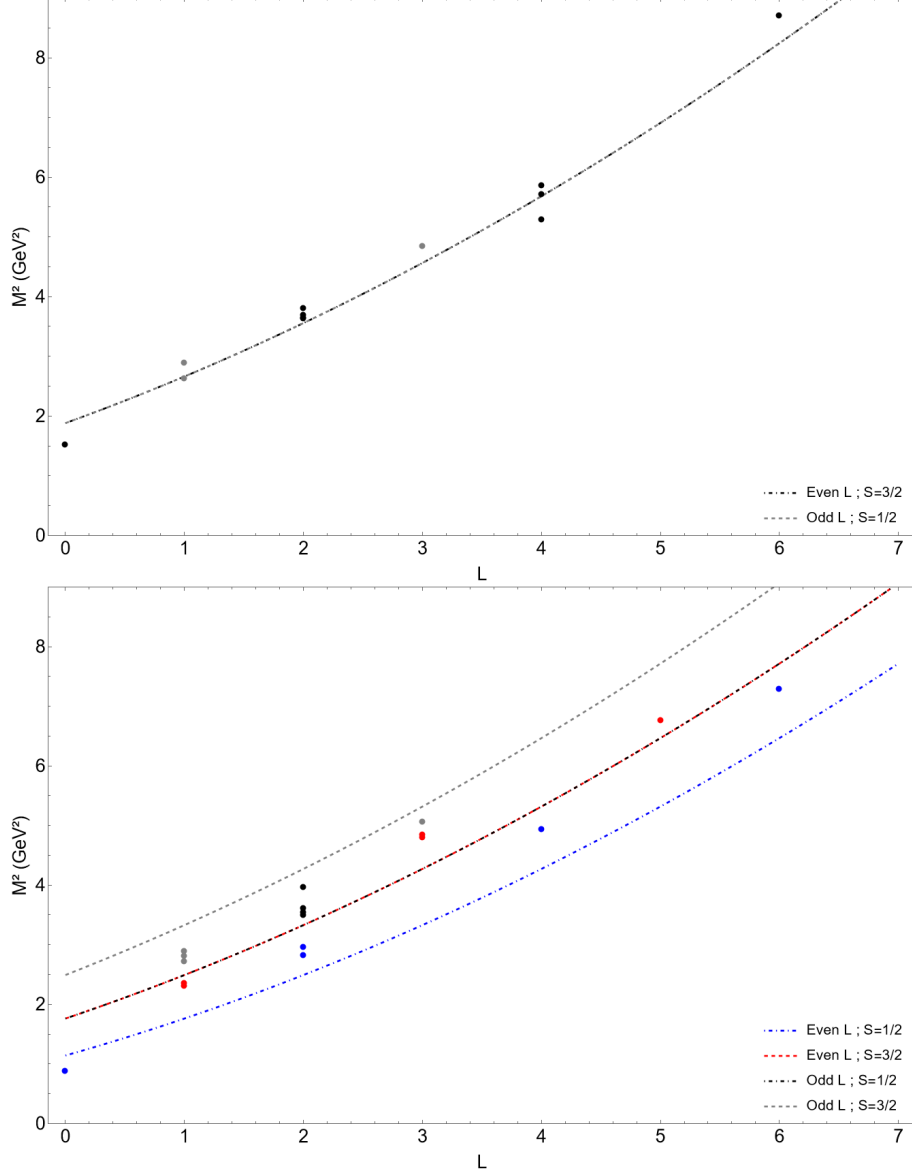


FIG. 1. Regge trajectories ( $M^2 \times L$ ) obtained from the HW model from equations (44)-(47), respectively with colors blue (dot-dashed), black(dot-dashed), red (dashed), and grey (dashed), for delta resonances (upper panel) and nucleon resonances (lower panel), with masses  $M$  expressed in GeV. As explained in the text, the delta resonances only present states with spin 1/2 with negative parity and spin 3/2 with positive parity, which in the HW are degenerate. Note that the trajectories corresponding to Eqs. (45) (black/dot-dashed) and (46) (red/dashed) coincide in both panels. We also present the corresponding experimental values (dots) obtained from the PDG. Each point of a given color corresponds to the trajectory of the same color.

available in PDG, for each model and particle family (nucleons and deltas). Note that the

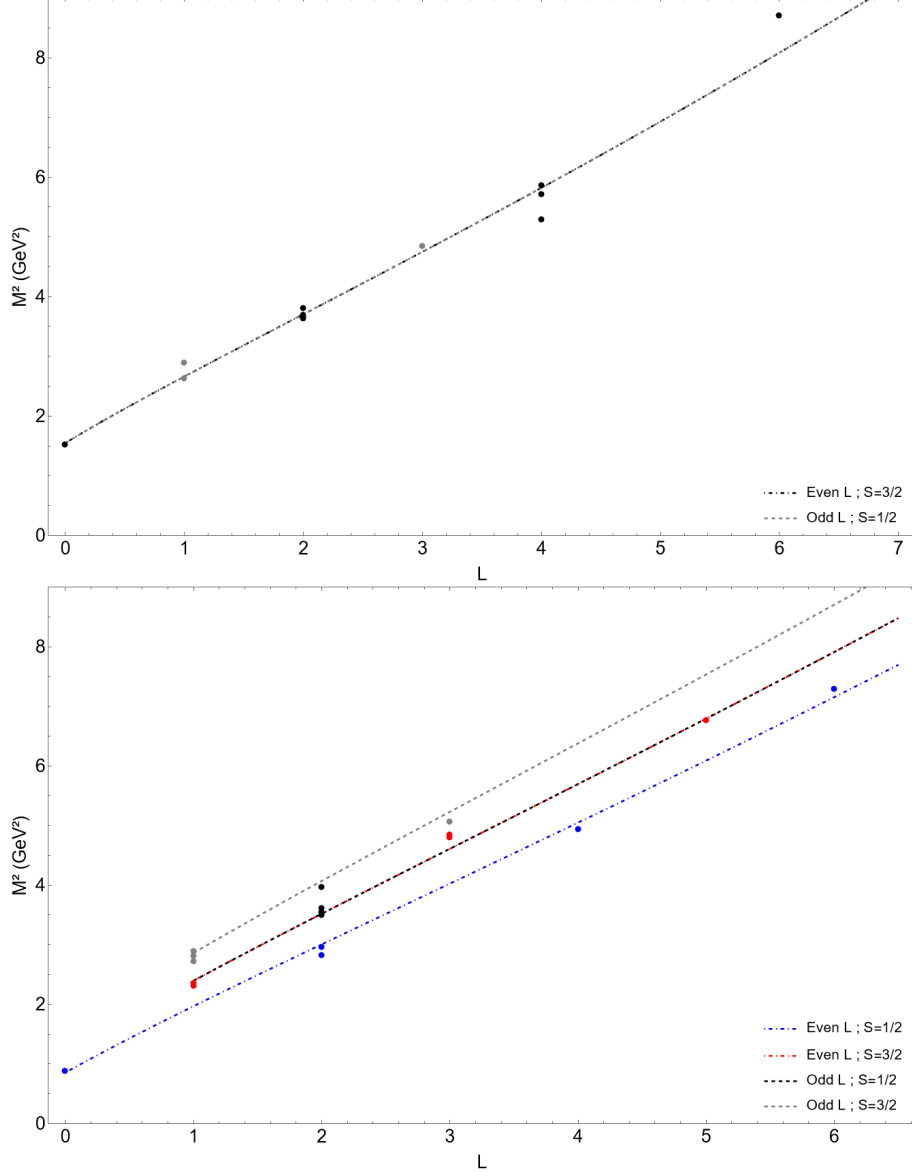


FIG. 2. Regge trajectories ( $M^2 \times L$ ) obtained from the AHW1 model, with anomalous dimension, Eq. (51), from equations (53)-(56), respectively with colors blue (dot-dashed), black(dot-dashed), red (dashed), and grey (dashed), for delta resonances (upper panel) and nucleon resonances (lower panel), with masses  $M$  expressed in GeV. As explained in the text, the delta resonances only present states with spin 1/2 with negative parity and spin 3/2 with positive parity, which in the AHW1 are degenerate. Note that the trajectories corresponding to Eqs. (54) (black/dot-dashed) and (55) (red/dashed) coincide in both panels. We also present the corresponding experimental values (dots) obtained from the PDG. Each point of a given color corresponds to the trajectory of the same color.

values of  $\Lambda$  found for the  $\text{AHW}_1$  for deltas and nucleons were also used in the  $\text{AHW}_2$ , for these families, for simplicity. In this table, one can see that the total deviation  $Q$  is smaller for the  $\text{AHW}_1$  model compared to the original HW and  $\text{AHW}_2$  models.

Family	Model	$\Lambda$ (MeV)	$a$	$b$	$Q/n$ %
Deltas	HW	215	-	-	(13.9/12)% = 1.16%
Nucleons	HW	208	-	-	(28.6/18)% = 1.59%
Deltas	$\text{AHW}_1$	151	1.74	1.55	(7.75/12)% = 0.646%
Nucleons	$\text{AHW}_1$	127	3.20	1.75	(8.61/18)% = 0.478%
Deltas	$\text{AHW}_2$	151	1.90	0.89	(17.1/12)% = 1.43%
Nucleons	$\text{AHW}_2$	127	2.82	1.69	(19.2/18)% = 1.07%

TABLE III. Values of the relevant parameters of the models HW,  $\text{AHW}_1$ , and  $\text{AHW}_2$  obtained by the minimization of  $Q$  function, Eq. (2). Notice that the HW model does not present  $a$  and  $b$  parameters. In the last column we present the value of the  $Q$  function over the  $n$  states used to construct such function.

In Tables IV and V, we present our results for the masses of the delta and nucleon resonances, respectively, for the HW,  $\text{AHW}_1$ , and  $\text{AHW}_2$  models. The first three columns of both tables show the orbital angular momentum excitation  $L$ , the parity  $P$ , and the spin  $S$ , of each state. The fourth column presents the corresponding masses of these states given by PDG. These Tables also present our results for the masses of these states obtained from the HW model, the  $\text{AHW}_1$  and  $\text{AHW}_2$ , as well as the percentage deviation of each of these masses compared to PDG. As anticipated in Table III, one can see in Tables IV and V that the masses obtained from the  $\text{AHW}_1$  for the delta and nucleon resonances have smaller deviations with respect to PDG data than the ones from the original HW and  $\text{AHW}_2$  models.

It is important to note that in equations (44)-(47) for the HW model, there are degeneracies in masses for different  $L$ , for example, for positive parity, with spin 1/2 and  $L = 2$  which presents the same mass as the negative parity, with spin 1/2 and  $L = 1$ . There are other degeneracies and they appear in the spectrum presented in Tables IV and V. Even

$L$	$P$	$S$	PDG	HW	$\delta_{\text{HW}}$	AHW <sub>1</sub>	$\delta_{\text{AHW}_1}$	AHW <sub>2</sub>	$\delta_{\text{AHW}_2}$
0	+	$\frac{3}{2}$	1232	1372	11.3	1244	1.01	1361	10.5
1	-	$\frac{1}{2}$	1620	1631	0.709	1632	0.731	1536	5.16
1	-	$\frac{1}{2}$	1700	1631	4.03	1632	4.01	1536	9.62
2	+	$\frac{3}{2}$	1910	1886	1.26	1925	0.778	1935	1.33
2	+	$\frac{3}{2}$	1920	1886	1.78	1925	0.253	1935	0.807
2	+	$\frac{3}{2}$	1905	1886	1.00	1925	1.04	1935	1.60
2	+	$\frac{3}{2}$	1950	1886	3.29	1925	1.29	1935	0.744
3	-	$\frac{1}{2}$	2200	2136	2.90	2179	0.936	2105	4.30
4	+	$\frac{3}{2}$	2390	2384	0.269	2413	0.955	2403	0.561
4	+	$\frac{3}{2}$	2300	2384	3.63	2413	4.90	2403	4.50
4	+	$\frac{3}{2}$	2420	2384	1.51	2413	0.297	2403	0.685
6	+	$\frac{3}{2}$	2950	2871	2.67	2843	3.62	2828	4.15

TABLE IV. Delta resonance states characterized by their orbital angular momentum  $L$ , parity  $P$ , and spin  $S$ , with their corresponding masses (in MeV) from PDG, and our results from the HW, Eqs. (44)-(47), and AHW<sub>1</sub> and AHW<sub>2</sub> models, Eqs. (53)-(56) with  $\Delta_{\text{anom.}}$  given by Eqs (51) and (52), respectively. For comparison, we also present the percentage deviation between these masses and the ones from PDG.

in the AHW<sub>1</sub> case, with equations (53)-(56), the same degeneracies arise. It is a feature of the model, but also expected, since for a given mass, there are states with different angular momentum: those who fall in the leading Regge trajectory and others in the daughters trajectories. For example, in Figures 2 and 8 of reference [136], we can also see this happening for delta and nucleon resonances, respectively.

Given the masses and, for example, the orbital angular momentum  $L$ , we can construct the Regge trajectory  $M^2 \times L$ . It is important to note that only states with positive parity and  $S = 3/2$  or negative parity and  $S = 1/2$  are known for delta resonances, so we will only construct Regge trajectories in delta cases for the observed states that are degenerated even in the original HW or in the AHW<sub>1</sub> and AHW<sub>2</sub> models. The "missing states" are discussed, for example, in [137].

In Figs. 1, 2, and 3, we present the Regge trajectories (dashed and dot-dashed lines)

$L$	$P$	$S$	PDG	HW	$\delta_{\text{HW}}$	AHW <sub>1</sub>	$\delta_{\text{AHW}_1}$	AHW <sub>2</sub>	$\delta_{\text{AHW}_2}$
0	+	$\frac{1}{2}$	939	1068	13.8	926	1.42	916	2.39
1	-	$\frac{1}{2}$	1520	1578	3.84	1548	1.84	1501	1.23
1	-	$\frac{1}{2}$	1535	1578	2.83	1548	0.846	1501	2.19
1	-	$\frac{3}{2}$	1650	1824	10.6	1691	2.51	1808	9.59
1	-	$\frac{3}{2}$	1700	1824	7.32	1691	0.504	1808	6.37
1	-	$\frac{3}{2}$	1675	1824	8.92	1691	0.981	1808	7.96
2	+	$\frac{1}{2}$	1720	1578	8.23	1734	0.808	1665	3.16
2	+	$\frac{1}{2}$	1680	1578	6.05	1734	3.21	1665	0.851
2	+	$\frac{3}{2}$	1880	1824	2.95	1876	0.210	1923	2.30
2	+	$\frac{3}{2}$	1900	1824	3.98	1876	1.26	1923	1.23
2	+	$\frac{3}{2}$	1870	1824	2.43	1876	0.324	1923	2.85
2	+	$\frac{3}{2}$	1990	1824	8.32	1876	5.72	1923	3.35
3	-	$\frac{1}{2}$	2190	2067	5.63	2147	1.97	2064	5.73
3	-	$\frac{1}{2}$	2220	2067	6.90	2147	3.29	2064	7.01
3	-	$\frac{3}{2}$	2250	2306	2.49	2247	1.64	2292	1.89
4	+	$\frac{1}{2}$	2220	2067	6.90	2606	1.21	2152	3.03
5	-	$\frac{1}{2}$	2600	2543	2.20	2606	0.244	2503	3.71
6	+	$\frac{1}{2}$	2700	2543	5.82	2675	0.939	2564	5.04

TABLE V. Nucleon resonance states characterized by their orbital angular momentum  $L$ , parity  $P$ , and spin  $S$ , with their corresponding masses (in MeV) from PDG, and our results from the HW, Eqs. (44)-(47), and AHW<sub>1</sub> and AHW<sub>2</sub> models, Eqs. (53)-(56) with  $\Delta_{\text{anom.}}$  given by Eqs (51) and (52), respectively. For comparison, we also present the percentage deviation between these masses and the ones from PDG.

obtained from the original HW, AHW<sub>1</sub> and AHW<sub>2</sub> models, respectively. In the upper panels, we show delta resonances and in the lower panels, nucleon resonances. In all panels, we also present the states obtained from PDG, which are represented by dots. Ideally, each dot of a given color would fall in the mass trajectory of the same color.

As a well-known result, the trajectories in the original HW model, Fig. 1, do not present the expected linear growth of  $M^2$  with  $L$ . On the other hand, in the trajectories obtained

from the  $AHW_1$  and  $AHW_2$  models, presented in Figs. 2, and 3, we can see improvements of two kinds with respect to the HW model: the first is that the masses of PDG lie much closer to the trajectories in these cases. The second is that these trajectories look much more linear.

Furthermore, in the case of Fig. 1, representing our results for the HW model, we can see from equations (45) and (46), the mass trajectory for spin  $S = 1/2$  and negative parity is degenerate with  $S = 3/2$  and positive parity, both for nucleons and deltas. A similar situation occurs for the  $AHW_1$  model with trajectories shown in Fig. 2. In this case, the degeneracy is related to Eqs. (54) and (55). A different behavior happens for the  $AHW_2$ , with trajectories represented in Fig. 3. In this case, there is no degeneracy between the trajectories, since the anomalous dimension given by Eq. (52), depends on the angular momentum  $L$  and the spin  $S$  of the states, and then these degeneracies are broken. So, there are no crossings between the trajectories in this case.

## V. LINEAR ANOMALOUS HARD WALL

An important fact about the Hard Wall model, and one that motivated the development of other holographic models, is that it presents non-linear Regge trajectories. As observed in the previous section, the anomalous models presented much more linear trajectories compared to the original HW model. Despite this, if we extrapolate the plots to observe higher values of angular momentum, we would observe a tendency towards non-linearity.

Based on previously developed ideas, [128, 129], we sought to determine if it is possible to obtain asymptotically linear Regge trajectories for baryons through direct modifications to the total mass dimension. As observed in previous works, a dimension of the type

$$\Delta_{\text{Lin.}} = aL^c + b, \tag{57}$$

leads to asymptotically linear trajectories for even-spin glueballs and light mesons, with  $c \approx 0.50$ . Here, for baryons, the Regge trajectories obtained are approximately linear for  $c \approx 0.75$ . A possible explanation is that even glueballs and mesons have two valence particles and in baryons three. So, it could be that one has to sum 0.25 for each valence parton inside the hadron to get a linear Regge trajectory in this model.

Taking into account the differences of the previous models with respect to the spin of the

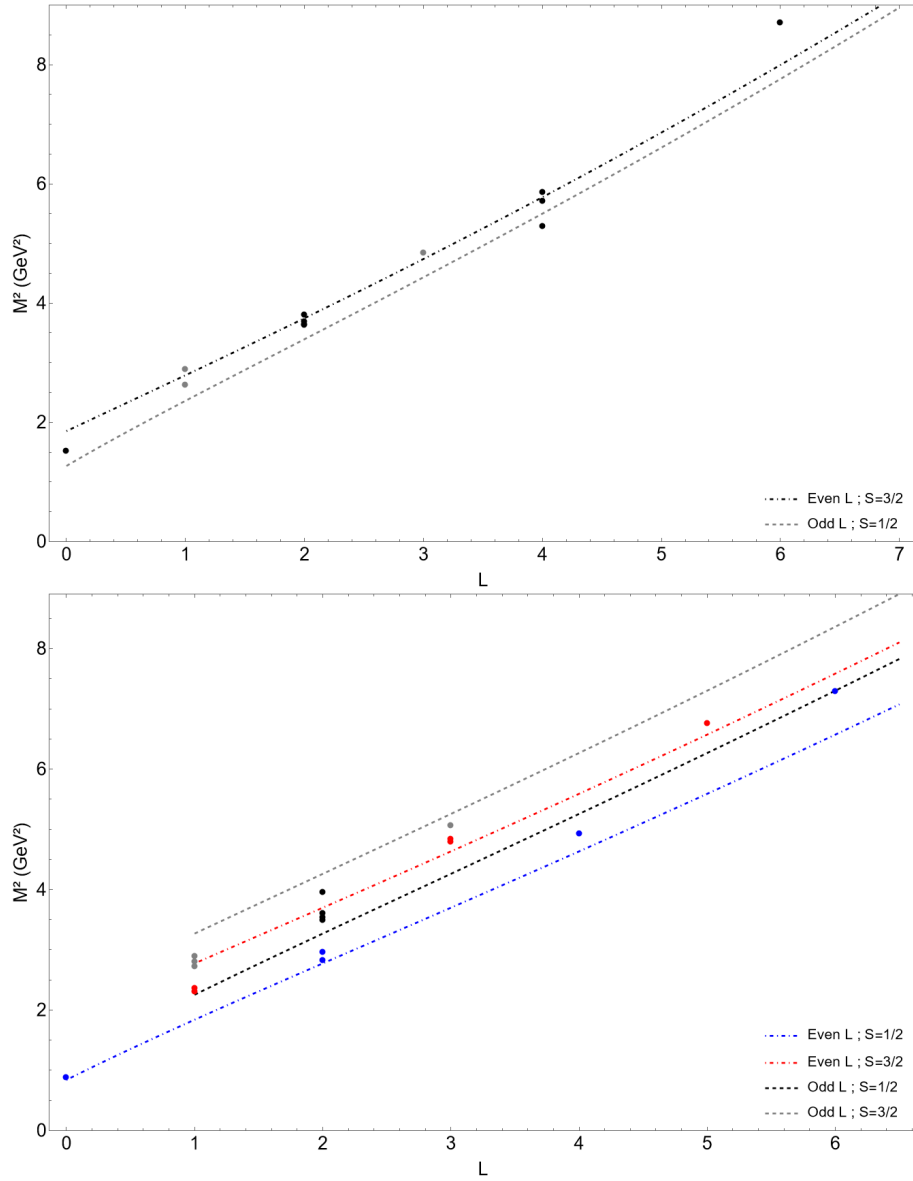


FIG. 3. Regge trajectories ( $M^2 \times L$ ) obtained from the AHW2 model, with anomalous dimension, Eq. (52), from equations (53)-(56), respectively with colors blue (dot-dashed), black(dot-dashed), red (dashed), and grey (dashed), for delta resonances (upper panel) and nucleon resonances (lower panel), with masses  $M$  expressed in GeV. As explained in the text, the delta resonances only present states with spin 1/2 with negative parity and spin 3/2 with positive parity. In both panels, we also present the corresponding experimental values (dots) obtained from the PDG. Each point of a given color corresponds to the trajectory of the same color.

resonances, in this model, we propose that the dimension of the baryonic operator is given

by

$$\Delta = \begin{cases} \frac{9}{2} + \Delta_{\text{Lin.}}; & S = 1/2, \\ \frac{11}{2} + \Delta_{\text{Lin.}}; & S = 3/2, \end{cases} \quad (58)$$

where  $S$  is the spin of the baryon.

As before, we can write the mass spectrum from the mass dimension of the operators, depending on the parity (whether it has even or odd angular momentum) and the spin. The masses of the positive-parity spin states  $1/2$  are then

$$M_{1/2+}(L) = \chi_{2+\Delta_{\text{Lin.}}} \Lambda_{\text{ALHW}}; \quad (\text{nucleons}), \quad (59)$$

and for negative parity,

$$M_{1/2-}(L) = \chi_{3+\Delta_{\text{Lin.}}} \Lambda_{\text{ALHW}}; \quad (\text{nucleons and deltas}). \quad (60)$$

For spin- $3/2$  and positive parity, we have

$$M_{3/2+}(L) = \chi_{3+\Delta_{\text{Lin.}}} \Lambda_{\text{ALHW}}; \quad (\text{nucleons and deltas}), \quad (61)$$

and for negative parity,

$$M_{3/2-}(L) = \chi_{4+\Delta_{\text{Lin.}}} \Lambda_{\text{ALHW}}; \quad (\text{nucleons}). \quad (62)$$

Minimizing the function  $Q$ , as in the previous section, to determine the values of the parameters  $a$  and  $b$ , and with an exponent around  $c \approx 0.75$ . Figure 4 shows the results obtained for the trajectories, and Table VI shows the values of the parameters obtained in this way.

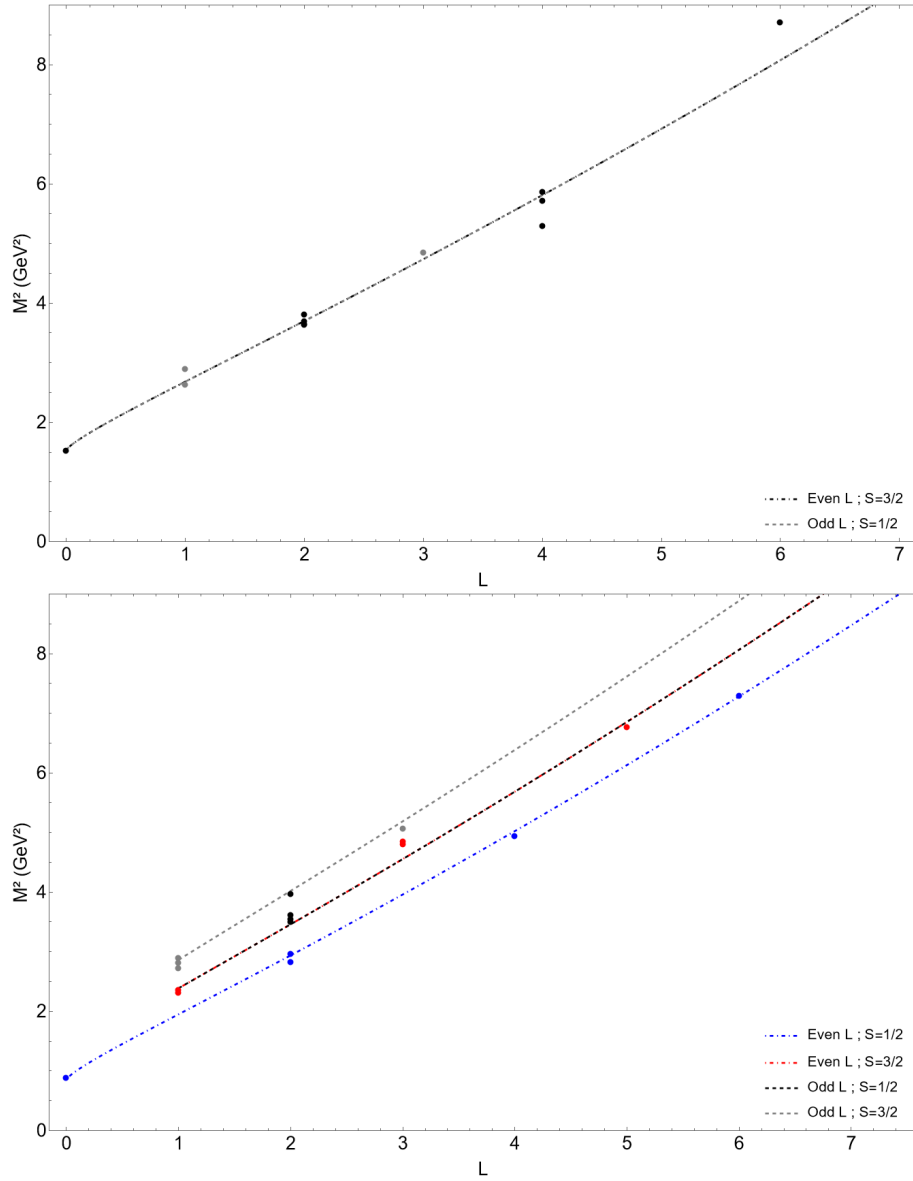


FIG. 4. Regge trajectories ( $L \times M^2$ ) for baryons, with masses  $M$  expressed in GeV, from the anomalous linear hard wall model, obtained from equations (59)-(62), respectively with colors blue (dot-dashed), black (dashed), red (dot-dashed), and grey (dashed). Note that the trajectories corresponding to Eqs. (60) (black) and (61) (red) coincide. *Upper panel*: Delta resonances; *Lower panel*: Nucleon resonances. In both cases, we also present the points corresponding to the experimental values obtained from the PDG. Each point of a given color corresponds to the trajectory of the same color.

Family	$\Lambda$ (MeV)	$a$	$b$	$c$	Q/n %
Deltas	113	3.12	3.90	0.79	(7.54/12)% = 0.628%
Nucleons	132	3.06	1.52	0.76	(9.12/18)% = 0.507%

TABLE VI. Values of the parameters for the anomalous linear hard wall model in equation (57) that minimizes the  $Q$  function, Eq. (2), for delta and nucleon resonances. The masses obtained in this model are presented in Tables VII and VIII, and the Regge trajectories in Fig. 4.

$L$	$P$	$S$	PDG	ALHW	$\delta_{\text{ALHW}}$
0	+	$\frac{3}{2}$	1232	1240	0.64
1	-	$\frac{1}{2}$	1620	1638	1.13
1	-	$\frac{1}{2}$	1700	1638	3.63
2	+	$\frac{3}{2}$	1910	1924	0.72
2	+	$\frac{3}{2}$	1920	1924	0.19
2	+	$\frac{3}{2}$	1905	1924	0.98
2	+	$\frac{3}{2}$	1950	1924	1.35
3	-	$\frac{1}{2}$	2200	2177	1.06
4	+	$\frac{3}{2}$	2390	2411	0.86
4	+	$\frac{3}{2}$	2300	2411	4.81
4	+	$\frac{3}{2}$	2420	2411	0.39
6	+	$\frac{3}{2}$	2950	2842	3.67

TABLE VII. Delta resonance states characterized by their orbital angular momentum  $L$ , parity  $P$ , and spin  $S$ , with their corresponding masses (in MeV) from PDG, and from the ALHW model, equations (59)-(62), with  $\Delta_{\text{Lin}}$  given by equation (57). For comparison, we also present the percentage deviation between the masses from this model and PDG.

$L$	$P$	$S$	PDG	ALHW	$\delta_{\text{ALHW}}$
0	+	$\frac{1}{2}$	939	926	1.43
1	-	$\frac{1}{2}$	1520	1551	2.02
1	-	$\frac{1}{2}$	1535	1551	1.03
1	-	$\frac{3}{2}$	1650	1700	3.05
1	-	$\frac{3}{2}$	1700	1700	0.018
1	-	$\frac{3}{2}$	1675	1700	1.51
2	+	$\frac{1}{2}$	1720	1718	0.088
2	+	$\frac{1}{2}$	1680	1718	2.29
2	+	$\frac{3}{2}$	1880	1867	0.70
2	+	$\frac{3}{2}$	1900	1867	1.75
2	+	$\frac{3}{2}$	1870	1867	0.17
2	+	$\frac{3}{2}$	1990	1867	6.19
3	-	$\frac{1}{2}$	2190	2142	2.21
3	-	$\frac{1}{2}$	2220	2142	3.53
3	-	$\frac{3}{2}$	2250	2288	1.67
4	+	$\frac{1}{2}$	2220	2247	1.23
5	-	$\frac{1}{2}$	2600	2627	1.05
6	+	$\frac{1}{2}$	2700	2706	0.22

TABLE VIII. Nucleon resonance states characterized by their orbital angular momentum  $L$ , parity  $P$ , and spin  $S$ , with their corresponding masses (in MeV) from PDG, and from the ALHW model, equations (59)-(62), with  $\Delta_{\text{Lin}}$  given by equation (57). For comparison, we also present the percentage deviation between the masses from this model and PDG.

## VI. DISCUSSION AND CONCLUSIONS

In this work, anomalous modifications of the original Hard Wall model were proposed to describe light baryons and obtain their spectra. We also presented the original Hard Wall model using different canonical dimensions for spin states  $S = 1/2$  and  $S = 3/2$ . The main objective of such changes was to obtain better outputs in comparison with previous results from the Hard Wall model for baryons.

Despite the fact that we obtain better results only by changing the canonical dimension, the HW model still presents non linear Regge trajectories and that was one of the reasons for considering the AHW models.

Inspired by the semiclassical approximation of the AdS/CFT correspondence for the anomalous dimension, given by Eq. (50), we proposed two models for our anomalous dimension. The first depends only on the orbital angular momentum, given by equation (51). This model allowed us to obtain approximate linear Regge trajectories and better masses for baryons if compared with PDG data. The second depends also on spin, equation (52). This model presents trajectories that are also more linear than the original hard wall, while the obtained masses are not as good as the first anomalous model. This comparison can be made more precise by looking at the values of  $Q/n$  in Table III, where the values are almost 50% better in  $AHW_1$  compared to  $AHW_2$ . If we compare the Regge trajectories of these models, in the first case the masses from PDG are in better agreement with the trajectories on which they should rely.

In addition, the linear realization of the anomalous dimension discussed in Section VI provides further insight into the asymptotic structure of the spectrum. In contrast to the purely logarithmic implementations, the linear correction improves the large-spin behavior of the Regge trajectories, yielding a more uniform spacing among highly excited states while preserving the overall consistency with the experimental data. Although this modification does not drastically alter the low-lying spectrum, it suggests that the functional form of the anomalous contribution plays a nontrivial role in controlling the asymptotic regime of the model. These results indicate that refining the scaling dimension beyond canonical values — particularly through simple power law deformations — may offer a promising direction for achieving a better holographic description of baryon Regge trajectories within the Hard Wall framework.

The possibility of a deeper physical motivation in the proposed anomalous linear model should be investigated in future work. Although it may not seem simple to demonstrate its phenomenological validity from first principles, we can perform an analysis, possibly studying objects with more valence quarks, such as tetraquarks and pentaquarks.

## ACKNOWLEDGMENTS

RACS is supported by Coordenação de Aperfeiçoamento de Pessoal de Nível Superior (CAPES). HBF is partially supported by Conselho Nacional de Desenvolvimento Científico e Tecnológico (CNPq) under grant 310346/2023-1, and Fundação Carlos Chagas Filho de Amparo à Pesquisa do Estado do Rio de Janeiro (FAPERJ) under grant E-26/204.095/2024.

---

## REFERENCES

- [1] F. Gross, E. Klempt, S. J. Brodsky, A. J. Buras, V. D. Burkert, G. Heinrich, K. Jakobs, C. A. Meyer, K. Orginos and M. Strickland, *et al.* “50 Years of Quantum Chromodynamics,” *Eur. Phys. J. C* **83**, 1125 (2023) doi:10.1140/epjc/s10052-023-11949-2 [arXiv:2212.11107 [hep-ph]].
- [2] E. Shuryak and I. Zahed, “The Hadron-Parton Bridge, From the QCD Vacuum to Partons,” [arXiv:2601.15085 [hep-ph]].
- [3] J. M. Maldacena, “The Large  $N$  limit of superconformal field theories and supergravity,” *Adv. Theor. Math. Phys.* **2**, 231-252 (1998) doi:10.4310/ATMP.1998.v2.n2.a1 [arXiv:hep-th/9711200 [hep-th]].
- [4] S. S. Gubser, I. R. Klebanov and A. M. Polyakov, *Phys. Lett. B* **428**, 105-114 (1998) doi:10.1016/S0370-2693(98)00377-3 [arXiv:hep-th/9802109 [hep-th]].
- [5] E. Witten, “Anti de Sitter space and holography,” *Adv. Theor. Math. Phys.* **2**, 253-291 (1998) doi:10.4310/ATMP.1998.v2.n2.a2 [arXiv:hep-th/9802150 [hep-th]].
- [6] O. Aharony, S. S. Gubser, J. M. Maldacena, H. Ooguri and Y. Oz, “Large  $N$  field theories, string theory and gravity,” *Phys. Rept.* **323**, 183-386 (2000) doi:10.1016/S0370-1573(99)00083-6 [arXiv:hep-th/9905111 [hep-th]].
- [7] M. Ammon and J. Erdmenger, “Gauge/gravity duality: Foundations and applica-

- tions,” Cambridge University Press, 2015, ISBN 978-1-107-01034-5, 978-1-316-23594-2  
doi:10.1017/CBO9780511846373
- [8] J. Zaanen, Y. W. Sun, Y. Liu and K. Schalm, “Holographic Duality in Condensed Matter Physics,” Cambridge Univ. Press, 2015, ISBN 978-1-107-08008-9  
doi:10.1017/CBO9781139942492
- [9] J. Polchinski and M. J. Strassler, “Hard scattering and gauge / string duality,” *Phys. Rev. Lett.* **88**, 031601 (2002) doi:10.1103/PhysRevLett.88.031601 [arXiv:hep-th/0109174 [hep-th]].
- [10] J. Polchinski and M. J. Strassler, “Deep inelastic scattering and gauge / string duality,” *JHEP* **05**, 012 (2003) doi:10.1088/1126-6708/2003/05/012 [arXiv:hep-th/0209211 [hep-th]].
- [11] H. Boschi-Filho and N. R. F. Braga, “Gauge / string duality and scalar glueball mass ratios,” *JHEP* **05**, 009 (2003) doi:10.1088/1126-6708/2003/05/009 [arXiv:hep-th/0212207 [hep-th]].
- [12] H. Boschi-Filho and N. R. F. Braga, “QCD / string holographic mapping and glueball mass spectrum,” *Eur. Phys. J. C* **32**, 529-533 (2004) doi:10.1140/epjc/s2003-01526-4 [arXiv:hep-th/0209080 [hep-th]].
- [13] G. F. de Teramond and S. J. Brodsky, “Hadronic spectrum of a holographic dual of QCD,” *Phys. Rev. Lett.* **94**, 201601 (2005) doi:10.1103/PhysRevLett.94.201601 [arXiv:hep-th/0501022 [hep-th]].
- [14] J. Erlich, E. Katz, D. T. Son and M. A. Stephanov, “QCD and a holographic model of hadrons,” *Phys. Rev. Lett.* **95**, 261602 (2005) doi:10.1103/PhysRevLett.95.261602 [arXiv:hep-ph/0501128 [hep-ph]].
- [15] H. Boschi-Filho, N. R. F. Braga and H. L. Carrion, “Glueball Regge trajectories from gauge/string duality and the Pomeron,” *Phys. Rev. D* **73**, 047901 (2006) doi:10.1103/PhysRevD.73.047901 [arXiv:hep-th/0507063 [hep-th]].
- [16] A. Karch, E. Katz, D. T. Son and M. A. Stephanov, “Linear confinement and AdS/QCD,” *Phys. Rev. D* **74**, 015005 (2006) doi:10.1103/PhysRevD.74.015005 [arXiv:hep-ph/0602229 [hep-ph]].
- [17] P. Colangelo, F. De Fazio, F. Giannuzzi, F. Jugeau and S. Nicotri, “Light scalar mesons in the soft-wall model of AdS/QCD,” *Phys. Rev. D* **78**, 055009 (2008) doi:10.1103/PhysRevD.78.055009 [arXiv:0807.1054 [hep-ph]].
- [18] H. Forkel, “Holographic glueball structure,” *Phys. Rev. D* **78**, 025001 (2008) doi:10.1103/PhysRevD.78.025001 [arXiv:0711.1179 [hep-ph]].

- [19] A. Vega and I. Schmidt, “Scalar hadrons in AdS(5) x S\*\*5,” Phys. Rev. D **78**, 017703 (2008) doi:10.1103/PhysRevD.78.017703 [arXiv:0806.2267 [hep-ph]].
- [20] S. S. Afonin, “Regge spectrum from holographic models inspired by OPE,” Phys. Lett. B **678**, 477-480 (2009) doi:10.1016/j.physletb.2009.06.071 [arXiv:0902.3959 [hep-ph]].
- [21] C. Wang, S. He, M. Huang, Q. S. Yan and Y. Yang, “Scalar Mesons and glueballs in Dp-Dq hard-wall models,” Chin. Phys. C **34**, 319-324 (2010) doi:10.1088/1674-1137/34/3/003 [arXiv:0902.0864 [hep-ph]].
- [22] H. C. Kim, Y. Kim and U. Yakhshiev, “Mesons and nucleons from holographic QCD in a unified approach,” JHEP **11**, 034 (2009) doi:10.1088/1126-6708/2009/11/034 [arXiv:0908.3406 [hep-ph]].
- [23] R. Alvares, C. Hoyos and A. Karch, “An improved model of vector mesons in holographic QCD,” Phys. Rev. D **84**, 095020 (2011) doi:10.1103/PhysRevD.84.095020 [arXiv:1108.1191 [hep-ph]].
- [24] E. Folco Capossoli and H. Boschi-Filho, “Odd spin glueball masses and the Odderon Regge trajectories from the holographic hardwall model,” Phys. Rev. D **88**, no.2, 026010 (2013) doi:10.1103/PhysRevD.88.026010 [arXiv:1301.4457 [hep-th]].
- [25] A. Gorsky, P. N. Kopnin and A. Krikun, “Baryon as dyonic instanton-II. Baryon mass versus chiral condensate,” Phys. Rev. D **89**, no.2, 026012 (2014) doi:10.1103/PhysRevD.89.026012 [arXiv:1309.3362 [hep-th]].
- [26] M. Harada, Y. L. Ma and S. Matsuzaki, “Chiral effective theories from holographic QCD with scalars,” Phys. Rev. D **89**, no.11, 115012 (2014) doi:10.1103/PhysRevD.89.115012 [arXiv:1404.4532 [hep-ph]].
- [27] E. F. Capossoli, J. P. M. Graça and H. Boschi-Filho, “AdS/QCD oddball masses and the odderon Regge trajectory from a twist-five operator approach,” Phys. Rev. D **105**, no.2, 026026 (2022) doi:10.1103/PhysRevD.105.026026 [arXiv:2110.12498 [hep-th]].
- [28] H. R. Grigoryan and A. V. Radyushkin, “Structure of vector mesons in holographic model with linear confinement,” Phys. Rev. D **76**, 095007 (2007) doi:10.1103/PhysRevD.76.095007 [arXiv:0706.1543 [hep-ph]].
- [29] H. J. Kwee and R. F. Lebed, “Pion form-factors in holographic QCD,” JHEP **01**, 027 (2008) doi:10.1088/1126-6708/2008/01/027 [arXiv:0708.4054 [hep-ph]].
- [30] H. R. Grigoryan and A. V. Radyushkin, “Pion form-factor in chiral limit of hard-wall

- AdS/QCD model,” *Phys. Rev. D* **76**, 115007 (2007) doi:10.1103/PhysRevD.76.115007 [arXiv:0709.0500 [hep-ph]].
- [31] H. J. Kwee and R. F. Lebed, “Pion Form Factor in Improved Holographic QCD Backgrounds,” *Phys. Rev. D* **77**, 115007 (2008) doi:10.1103/PhysRevD.77.115007 [arXiv:0712.1811 [hep-ph]].
- [32] G. M. Huber *et al.* [Jefferson Lab], “Charged pion form-factor between  $Q^{*2} = 0.60\text{-GeV}^{*2}$  and  $2.45\text{-GeV}^{*2}$ . II. Determination of, and results for, the pion form-factor,” *Phys. Rev. C* **78**, 045203 (2008) doi:10.1103/PhysRevC.78.045203 [arXiv:0809.3052 [nucl-ex]].
- [33] P. Colangelo, J. J. Sanz-Cillero and F. Zuo, “Holography, chiral Lagrangian and form factor relations,” *JHEP* **11**, 012 (2012) doi:10.1007/JHEP11(2012)012 [arXiv:1207.5744 [hep-ph]].
- [34] S. Mamedov, B. B. Sirvanli, I. Atayev and N. Huseynova, “Nucleon’s axial-vector form factor in the hard-wall AdS/QCD model,” *Int. J. Theor. Phys.* **56**, no.6, 1861-1874 (2017) doi:10.1007/s10773-017-3330-x [arXiv:1609.00167 [hep-th]].
- [35] A. Ballon-Bayona, G. Krein and C. Miller, “Strong couplings and form factors of charmed mesons in holographic QCD,” *Phys. Rev. D* **96**, no.1, 014017 (2017) doi:10.1103/PhysRevD.96.014017 [arXiv:1702.08417 [hep-ph]].
- [36] M. A. Martin Contreras and A. Vega, “Different approach to decay constants in AdS/QCD models,” *Phys. Rev. D* **101**, no.4, 046009 (2020) doi:10.1103/PhysRevD.101.046009 [arXiv:1910.10922 [hep-th]].
- [37] S. Momeni and M. Saghebfar, “Charm meson couplings in Hard-Wall holographic QCD,” *Eur. Phys. J. C* **81**, no.2, 102 (2021) [erratum: *Eur. Phys. J. C* **82**, no.8, 709 (2022)] doi:10.1140/epjc/s10052-021-08870-x [arXiv:2007.02273 [hep-ph]].
- [38] C. A. Ballon Bayona, H. Boschi-Filho and N. R. F. Braga, “Deep inelastic scattering from gauge string duality in the soft wall model,” *JHEP* **03**, 064 (2008) doi:10.1088/1126-6708/2008/03/064 [arXiv:0711.0221 [hep-th]].
- [39] C. A. Ballon Bayona, H. Boschi-Filho and N. R. F. Braga, “Deep inelastic structure functions from supergravity at small  $x$ ,” *JHEP* **10**, 088 (2008) doi:10.1088/1126-6708/2008/10/088 [arXiv:0712.3530 [hep-th]].
- [40] C. A. B. Bayona, H. Boschi-Filho and N. R. F. Braga, “Holographic model for dilepton production in p-p collisions,” *Nucl. Phys. B* **851**, 66-85 (2011) doi:10.1016/j.nuclphysb.2011.05.010 [arXiv:1007.4362 [hep-th]].

- [41] R. Nishio and T. Watari, “Investigating Generalized Parton Distribution in Gravity Dual,” *Phys. Lett. B* **707**, 362-368 (2012) doi:10.1016/j.physletb.2011.12.051 [arXiv:1105.2907 [hep-ph]].
- [42] R. Nishio and T. Watari, “High-Energy Photon-Hadron Scattering in Holographic QCD,” *Phys. Rev. D* **84**, 075025 (2011) doi:10.1103/PhysRevD.84.075025 [arXiv:1105.2999 [hep-ph]].
- [43] R. C. Brower, M. Djuric and C. I. Tan, “Diffractive Higgs Production by AdS Pomeron Fusion,” *JHEP* **09**, 097 (2012) doi:10.1007/JHEP09(2012)097 [arXiv:1202.4953 [hep-ph]].
- [44] S. Bolognesi, J. N. Laia, D. Tong and K. Wong, “A Gapless Hard Wall: Magnetic Catalysis in Bulk and Boundary,” *JHEP* **07**, 162 (2012) doi:10.1007/JHEP07(2012)162 [arXiv:1204.6029 [hep-th]].
- [45] A. Watanabe and K. Suzuki, “Transition from soft- to hard-Pomeron in the structure functions of hadrons at small- $x$  from holography,” *Phys. Rev. D* **86**, 035011 (2012) doi:10.1103/PhysRevD.86.035011 [arXiv:1206.0910 [hep-ph]].
- [46] M. S. Costa, M. Djurić and N. Evans, “Vector meson production at low  $x$  from gauge/gravity duality,” *JHEP* **09**, 084 (2013) doi:10.1007/JHEP09(2013)084 [arXiv:1307.0009 [hep-ph]].
- [47] A. Watanabe and K. Suzuki, “Nucleon structure functions at small  $x$  via the Pomeron exchange in AdS space with a soft infrared wall,” *Phys. Rev. D* **89**, no.11, 115015 (2014) doi:10.1103/PhysRevD.89.115015 [arXiv:1312.7114 [hep-ph]].
- [48] L. Agozzino, P. Castorina and P. Colangelo, “Nuclear structure functions at low- $x$  in a holographic approach,” *Eur. Phys. J. C* **74**, no.4, 2828 (2014) doi:10.1140/epjc/s10052-014-2828-0 [arXiv:1401.0826 [hep-ph]].
- [49] M. Dehghani, “Hard-gluon Evolution of Nucleon Generalized Parton Distributions in Soft-Wall AdS/QCD Model,” *Phys. Rev. D* **91**, no.7, 076009 (2015) doi:10.1103/PhysRevD.91.076009 [arXiv:1501.02318 [hep-ph]].
- [50] E. Folco Capossoli and H. Boschi-Filho, “Deep Inelastic Scattering in the Exponentially Small Bjorken Parameter Regime from the Holographic Softwall Model,” *Phys. Rev. D* **92**, no.12, 126012 (2015) doi:10.1103/PhysRevD.92.126012 [arXiv:1509.01761 [hep-th]].
- [51] N. Kovensky, G. Michalski and M. Schvellinger, “Deep inelastic scattering from polarized spin-1/2 hadrons at low  $x$  from string theory,” *JHEP* **10**, 084 (2018) doi:10.1007/JHEP10(2018)084 [arXiv:1807.11540 [hep-th]].
- [52] W. Xie, A. Watanabe and M. Huang, “Elastic proton-proton scattering at LHC energies in

- holographic QCD,” *JHEP* **10**, 053 (2019) doi:10.1007/JHEP10(2019)053 [arXiv:1901.09564 [hep-ph]].
- [53] K. A. Mamo and I. Zahed, “Neutrino-nucleon DIS from holographic QCD: PDFs of sea and valence quarks, form factors, and structure functions of the proton,” *Phys. Rev. D* **104**, no.6, 066010 (2021) doi:10.1103/PhysRevD.104.066010 [arXiv:2102.00608 [hep-ph]].
- [54] M. Ghodrati, “String scattering amplitudes and mutual information in confining backgrounds: The partonic behavior,” *Phys. Rev. D* **112**, no.4, 046011 (2025) doi:10.1103/mv9d-kmq4 [arXiv:2307.13454 [hep-th]].
- [55] A. Armoni, B. Pyszkowski and D. Weissman, “High-Energy Pion Scattering in Holographic QCD: A Comparison with Experimental Data,” [arXiv:2512.18274 [hep-ph]].
- [56] H. Boschi-Filho, N. R. F. Braga and C. N. Ferreira, “Static strings in Randall-Sundrum scenarios and the quark anti-quark potential,” *Phys. Rev. D* **73**, 106006 (2006) [erratum: *Phys. Rev. D* **74**, 089903 (2006)] doi:10.1103/PhysRevD.74.089903 [arXiv:hep-th/0512295 [hep-th]].
- [57] O. Andreev and V. I. Zakharov, “Heavy-quark potentials and AdS/QCD,” *Phys. Rev. D* **74**, 025023 (2006) doi:10.1103/PhysRevD.74.025023 [arXiv:hep-ph/0604204 [hep-ph]].
- [58] C. D. White, “The Cornell potential from general geometries in AdS / QCD,” *Phys. Lett. B* **652**, 79-85 (2007) doi:10.1016/j.physletb.2007.07.006 [arXiv:hep-ph/0701157 [hep-ph]].
- [59] R. C. L. Bruni, E. Folco Capossoli and H. Boschi-Filho, “Quark-antiquark potential from a deformed AdS/QCD,” *Adv. High Energy Phys.* **2019**, 1901659 (2019) doi:10.1155/2019/1901659 [arXiv:1806.05720 [hep-th]].
- [60] U. Gursoy and E. Kiritsis, “Exploring improved holographic theories for QCD: Part I,” *JHEP* **02**, 032 (2008) doi:10.1088/1126-6708/2008/02/032 [arXiv:0707.1324 [hep-th]].
- [61] U. Gursoy, E. Kiritsis and F. Nitti, “Exploring improved holographic theories for QCD: Part II,” *JHEP* **02**, 019 (2008) doi:10.1088/1126-6708/2008/02/019 [arXiv:0707.1349 [hep-th]].
- [62] W. de Paula, T. Frederico, H. Forkel and M. Beyer, “Dynamical AdS/QCD with area-law confinement and linear Regge trajectories,” *Phys. Rev. D* **79**, 075019 (2009) doi:10.1103/PhysRevD.79.075019 [arXiv:0806.3830 [hep-ph]].
- [63] D. Li and M. Huang, “Dynamical holographic QCD model for glueball and light meson spectra,” *JHEP* **11**, 088 (2013) doi:10.1007/JHEP11(2013)088 [arXiv:1303.6929 [hep-ph]].
- [64] E. Folco Capossoli and H. Boschi-Filho, “Glueball spectra and Regge trajectories

- from a modified holographic softwall model,” *Phys. Lett. B* **753**, 419-423 (2016) doi:10.1016/j.physletb.2015.12.034 [arXiv:1510.03372 [hep-ph]].
- [65] E. Folco Capossoli, D. Li and H. Boschi-Filho, “Pomeron and Odderon Regge Trajectories from a Dynamical Holographic Model,” *Phys. Lett. B* **760**, 101-105 (2016) doi:10.1016/j.physletb.2016.06.049 [arXiv:1601.05114 [hep-ph]].
- [66] D. M. Rodrigues, E. Folco Capossoli and H. Boschi-Filho, “Scalar and higher even spin glueball masses from an anomalous modified holographic model,” *EPL* **122**, no.2, 21001 (2018) doi:10.1209/0295-5075/122/21001 [arXiv:1611.09817 [hep-ph]].
- [67] A. Ballon-Bayona and L. A. H. Mamani, “Nonlinear realization of chiral symmetry breaking in holographic soft wall models,” *Phys. Rev. D* **102**, no.2, 026013 (2020) doi:10.1103/PhysRevD.102.026013 [arXiv:2002.00075 [hep-ph]].
- [68] O. Andreev and V. I. Zakharov, “The Spatial String Tension, Thermal Phase Transition, and AdS/QCD,” *Phys. Lett. B* **645**, 437-441 (2007) doi:10.1016/j.physletb.2007.01.002 [arXiv:hep-ph/0607026 [hep-ph]].
- [69] H. Boschi-Filho, N. R. F. Braga and C. N. Ferreira, “Heavy quark potential at finite temperature from gauge/string duality,” *Phys. Rev. D* **74**, 086001 (2006) doi:10.1103/PhysRevD.74.086001 [arXiv:hep-th/0607038 [hep-th]].
- [70] C. P. Herzog, “A Holographic Prediction of the Deconfinement Temperature,” *Phys. Rev. Lett.* **98**, 091601 (2007) doi:10.1103/PhysRevLett.98.091601 [arXiv:hep-th/0608151 [hep-th]].
- [71] C. A. Ballon Bayona, H. Boschi-Filho, N. R. F. Braga and L. A. Pando Zayas, “On a Holographic Model for Confinement/Deconfinement,” *Phys. Rev. D* **77**, 046002 (2008) doi:10.1103/PhysRevD.77.046002 [arXiv:0705.1529 [hep-th]].
- [72] R. G. Cai and J. P. Shock, “Holographic confinement/deconfinement phase transitions of AdS/QCD in curved spaces,” *JHEP* **08**, 095 (2007) doi:10.1088/1126-6708/2007/08/095 [arXiv:0705.3388 [hep-th]].
- [73] U. Gursoy, “Deconfinement and Thermodynamics in 5D Holographic Models of QCD,” *Mod. Phys. Lett. A* **23**, 3349-3365 (2009) doi:10.1142/S0217732308029940 [arXiv:0904.2750 [hep-th]].
- [74] A. S. Miranda, C. A. Ballon Bayona, H. Boschi-Filho and N. R. F. Braga, “Black-hole quasinormal modes and scalar glueballs in a finite-temperature AdS/QCD model,” *JHEP* **2009**, no.11, 119 (2009) doi:10.1088/1126-6708/2009/11/119 [arXiv:0909.1790 [hep-th]].

- [75] L. A. H. Mamani, A. S. Miranda, H. Boschi-Filho and N. R. F. Braga, “Vector meson quasinormal modes in a finite-temperature AdS/QCD model,” *JHEP* **2014**, no.3, 58 (2014) doi:10.1007/JHEP03(2014)058 [arXiv:1312.3815 [hep-th]].
- [76] L. A. H. Mamani, A. S. Miranda and V. T. Zanchin, “Melting of scalar mesons and black-hole quasinormal modes in a holographic QCD model,” *Eur. Phys. J. C* **79**, no.5, 1-20 (2019) doi:10.1140/epjc/s10052-019-6902-5 [arXiv:1809.03508 [hep-th]].
- [77] N. R. F. Braga and O. C. Junqueira, “Configuration entropy and confinement /deconfinement transition in holographic QCD,” *Phys. Lett. B* **814**, 136082 (2021) doi:10.1016/j.physletb.2021.136082 [arXiv:2010.00714 [hep-th]].
- [78] C. O. Lee, “Configuration entropy and confinement-deconfinement transition in higher-dimensional hard wall model,” *Phys. Lett. B* **824**, 136851 (2022) doi:10.1016/j.physletb.2021.136851 [arXiv:2111.04111 [hep-th]].
- [79] A. Singh and K. P. Yogendran, “Phases of a 10-D holographic hard wall model,” *JHEP* **02**, 168 (2023) doi:10.1007/JHEP02(2023)168 [arXiv:2208.09387 [hep-th]].
- [80] P. Colangelo, F. Giannuzzi and S. Nicotri, “Holographic Approach to Finite Temperature QCD: The Case of Scalar Glueballs and Scalar Mesons,” *Phys. Rev. D* **80**, 094019 (2009) doi:10.1103/PhysRevD.80.094019 [arXiv:0909.1534 [hep-ph]].
- [81] K. Jo, B. H. Lee, C. Park and S. J. Sin, “Holographic QCD in medium: A Bottom up approach,” *JHEP* **06**, 022 (2010) doi:10.1007/JHEP06(2010)022 [arXiv:0909.3914 [hep-ph]].
- [82] B. Craps, E. Kiritsis, C. Rosen, A. Taliotis, J. Vanhoof and H. b. Zhang, “Gravitational collapse and thermalization in the hard wall model,” *JHEP* **02**, 120 (2014) doi:10.1007/JHEP02(2014)120 [arXiv:1311.7560 [hep-th]].
- [83] M. Rinaldi and V. Vento, “Glueballs at high temperature within the hard-wall holographic model,” *Eur. Phys. J. C* **82**, no.2, 140 (2022) doi:10.1140/epjc/s10052-022-10105-6 [arXiv:2112.11307 [hep-ph]].
- [84] L. Bartolini, S. B. Gudnason, J. Leutgeb and A. Rebhan, “Neutron stars and phase diagram in a hard-wall AdS/QCD model,” *Phys. Rev. D* **105**, no.12, 126014 (2022) doi:10.1103/PhysRevD.105.126014 [arXiv:2202.12845 [hep-th]].
- [85] N. R. F. Braga, L. F. Faulhaber and O. C. Junqueira, “Confinement-deconfinement temperature for a rotating quark-gluon plasma,” *Phys. Rev. D* **105**, no.10, 106003 (2022) doi:10.1103/PhysRevD.105.106003 [arXiv:2201.05581 [hep-th]].

- [86] M. Rinaldi and V. Vento, “Phase transition in the holographic hard-wall model,” *Phys. Rev. D* **108**, no.11, 114020 (2023) doi:10.1103/PhysRevD.108.114020 [arXiv:2304.01793 [hep-ph]].
- [87] Z. C. Chen, S. L. Li, P. Wu and H. Yu, “NANOGrav hints for first-order confinement-deconfinement phase transition in different QCD-matter scenarios,” *Phys. Rev. D* **109**, no.4, 4 (2024) doi:10.1103/PhysRevD.109.043022 [arXiv:2312.01824 [astro-ph.CO]].
- [88] J. H. Wang and S. Q. Feng, “Rotation effect on the deconfinement phase transition in holographic QCD,” *Phys. Rev. D* **109**, no.6, 066019 (2024) doi:10.1103/PhysRevD.109.066019 [arXiv:2403.01814 [hep-ph]].
- [89] N. R. F. Braga and O. C. Junqueira, “Holographic QCD phase diagram for a rotating plasma in the Hawking-Page approach,” *Phys. Lett. B* **868**, 139669 (2025) doi:10.1016/j.physletb.2025.139669 [arXiv:2501.16446 [hep-th]].
- [90] N. Nasibova and X. D. Arsiwalla, “Pion phenomenology from the thermal soft-wall model of holographic QCD,” *Phys. Rev. D* **112**, no.11, 116010 (2025) doi:10.1103/m327-xs85 [arXiv:2505.23455 [hep-ph]].
- [91] D. Fujii, A. Hosaka, A. Iwanaka, T. Sakai and M. Tachibana, “Dense matter in a holographic hard-wall model of QCD,” *Phys. Rev. D* **113**, no.3, 034003 (2026) doi:10.1103/cssg-bqmc [arXiv:2506.06997 [hep-ph]].
- [92] A. Gorsky and A. Krikun, “Magnetic susceptibility of the quark condensate via holography,” *Phys. Rev. D* **79**, 086015 (2009) doi:10.1103/PhysRevD.79.086015 [arXiv:0902.1832 [hep-ph]].
- [93] Y. Y. Bu, J. Erdmenger, J. P. Shock and M. Strydom, “Magnetic field induced lattice ground states from holography,” *JHEP* **03**, 165 (2013) doi:10.1007/JHEP03(2013)165 [arXiv:1210.6669 [hep-th]].
- [94] K. A. Mamo, “Inverse magnetic catalysis in holographic models of QCD,” *JHEP* **05**, 121 (2015) doi:10.1007/JHEP05(2015)121 [arXiv:1501.03262 [hep-th]].
- [95] D. Dudal, D. R. Granado and T. G. Mertens, “No inverse magnetic catalysis in the QCD hard and soft wall models,” *Phys. Rev. D* **93**, no.12, 125004 (2016) doi:10.1103/PhysRevD.93.125004 [arXiv:1511.04042 [hep-th]].
- [96] D. M. Rodrigues, E. Folco Capossoli and H. Boschi-Filho, “Magnetic catalysis and inverse magnetic catalysis in (2+1)-dimensional gauge theories from holographic models,” *Phys. Rev. D* **97**, no.12, 126001 (2018) doi:10.1103/PhysRevD.97.126001 [arXiv:1710.07310 [hep-th]].

- [97] D. M. Rodrigues, E. Folco Capossoli and H. Boschi-Filho, “Deconfinement phase transition in a magnetic field in  $2 + 1$  dimensions from holographic models,” *Phys. Lett. B* **780**, 37-40 (2018) doi:10.1016/j.physletb.2018.02.049 [arXiv:1709.09258 [hep-th]].
- [98] D. M. Rodrigues, D. Li, E. Folco Capossoli and H. Boschi-Filho, “Chiral symmetry breaking and restoration in  $2+1$  dimensions from holography: Magnetic and inverse magnetic catalysis,” *Phys. Rev. D* **98**, no.10, 106007 (2018) doi:10.1103/PhysRevD.98.106007 [arXiv:1807.11822 [hep-th]].
- [99] D. M. Rodrigues, D. Li, E. Folco Capossoli and H. Boschi-Filho, “Holographic Description of Chiral Symmetry Breaking in a Magnetic Field in  $2+1$  Dimensions with an Improved Dilaton,” *EPL* **128**, no.6, 61001 (2019) doi:10.1209/0295-5075/128/61001 [arXiv:1811.04117 [hep-ph]].
- [100] J. L. F. Barbon and C. A. Fuertes, “A Note on the extensivity of the holographic entanglement entropy,” *JHEP* **05**, 053 (2008) doi:10.1088/1126-6708/2008/05/053 [arXiv:0801.2153 [hep-th]].
- [101] S. Grienering, D. E. Kharzeev and I. Zahed, “Entanglement in a holographic Schwinger pair with confinement,” *Phys. Rev. D* **108**, no.8, 086030 (2023) doi:10.1103/PhysRevD.108.086030 [arXiv:2305.07121 [hep-th]].
- [102] D. Gazit and H. U. Yee, “Weak-Interacting Holographic QCD,” *Phys. Lett. B* **670**, 154-160 (2008) doi:10.1016/j.physletb.2008.10.045 [arXiv:0807.0607 [hep-th]].
- [103] D. D. Dietrich and C. Kouvaris, “Generalised bottom-up holography and walking technicolour,” *Phys. Rev. D* **79**, 075004 (2009) doi:10.1103/PhysRevD.79.075004 [arXiv:0809.1324 [hep-ph]].
- [104] D. D. Dietrich, M. Jarvinen and C. Kouvaris, “Mixing in the axial sector in bottom-up holography for walking technicolour,” *JHEP* **07**, 023 (2010) doi:10.1007/JHEP07(2010)023 [arXiv:0908.4357 [hep-ph]].
- [105] D. Kutasov, J. Lin and A. Parnachev, “Holographic Walking from Tachyon DBI,” *Nucl. Phys. B* **863**, 361-397 (2012) doi:10.1016/j.nuclphysb.2012.05.025 [arXiv:1201.4123 [hep-th]].
- [106] D. K. Hong and D. Kim, “Pseudo scalar contributions to light-by-light correction of muon  $g-2$  in AdS/QCD,” *Phys. Lett. B* **680**, 480-484 (2009) doi:10.1016/j.physletb.2009.09.026 [arXiv:0904.4042 [hep-ph]].
- [107] J. Leutgeb and A. Rebhan, “Axial vector transition form factors in holographic QCD and

- their contribution to the anomalous magnetic moment of the muon,” *Phys. Rev. D* **101**, no.11, 114015 (2020) doi:10.1103/PhysRevD.101.114015 [arXiv:1912.01596 [hep-ph]].
- [108] P. Colangelo, F. Giannuzzi and S. Nicotri, “Hadronic light-by-light scattering contributions to  $(g-2)_\mu$  from axial-vector and tensor mesons in the holographic soft-wall model,” *Phys. Rev. D* **109**, no.9, 9 (2024) doi:10.1103/PhysRevD.109.094036 [arXiv:2402.07579 [hep-ph]].
- [109] J. Mager, L. Cappiello, J. Leutgeb and A. Rebhan, “Longitudinal Short-Distance Constraints on Hadronic Light-by-Light Scattering and Tensor-Meson Contributions to the Muon  $g-2$ ,” *Phys. Rev. Lett.* **135**, no.9, 091901 (2025) doi:10.1103/dxwr-gpsl [arXiv:2501.19293 [hep-ph]].
- [110] J. Y. Shen, W. Y. Peng, L. Y. Dai and Z. Fang, “Hadronic Contributions to the Muon  $g - 2$  in Improved Holographic QCD Models,” [arXiv:2602.23590 [hep-ph]].
- [111] L. Cappiello and G. D’Ambrosio, “On the Evaluation of Gluon Condensate Effects in the Holographic Approach to QCD,” *Eur. Phys. J. C* **69**, 315-329 (2010) doi:10.1140/epjc/s10052-010-1386-3 [arXiv:0912.3721 [hep-ph]].
- [112] D. Albrecht and J. Erlich, “Pion condensation in holographic QCD,” *Phys. Rev. D* **82**, 095002 (2010) doi:10.1103/PhysRevD.82.095002 [arXiv:1007.3431 [hep-ph]].
- [113] Y. Chen, M. Ding, D. Li, K. Bitaghsir Fadafan and M. Huang, “Pion condensation and pion star from holographic QCD,” *Phys. Rev. D* **111**, no.12, 126010 (2025) doi:10.1103/94zt-q2dw [arXiv:2408.17080 [hep-ph]].
- [114] B. H. Lee, C. Park and S. Shin, “Holographic  $1/N_c$  correction from the chiral condensate,” *JHEP* **12**, 071 (2010) doi:10.1007/JHEP12(2010)071 [arXiv:1010.1109 [hep-th]].
- [115] Y. Z. Li, “Effective field theory bootstrap, large- $N$   $\chi$ PT and holographic QCD,” *JHEP* **01**, 072 (2024) doi:10.1007/JHEP01(2024)072 [arXiv:2310.09698 [hep-th]].
- [116] Y. Kim and D. Yi, “Holography at work for nuclear and hadron physics,” *Adv. High Energy Phys.* **2011**, 259025 (2011) doi:10.1155/2011/259025 [arXiv:1107.0155 [hep-ph]].
- [117] C. Park, “Holographic Symmetry Energy of the Nuclear Matter,” *Phys. Lett. B* **708**, 324-329 (2012) doi:10.1016/j.physletb.2012.01.057 [arXiv:1112.0386 [hep-th]].
- [118] L. Agozzino, P. Castorina and P. Colangelo, “Nuclear Shadowing in the Holographic Framework,” *Phys. Rev. Lett.* **112**, no.4, 041601 (2014) doi:10.1103/PhysRevLett.112.041601 [arXiv:1306.5072 [hep-ph]].
- [119] C. Park, “Meson’s Correlation Functions in a Nuclear Medium,” *Phys. Lett. B* **760**, 79-85 (2016) doi:10.1016/j.physletb.2016.06.043 [arXiv:1603.04101 [hep-th]].

- [120] M. A. Martin Contreras, A. Vega and S. Diles, “A holographic bottom-up description of light nuclide spectroscopy and stability,” *Phys. Lett. B* **835**, 137551 (2022) doi:10.1016/j.physletb.2022.137551 [arXiv:2206.01834 [hep-ph]].
- [121] V. G. M. Puletti, S. Nowling, L. Thorlacius and T. Zingg, “Friedel Oscillations in Holographic Metals,” *JHEP* **01**, 073 (2012) doi:10.1007/JHEP01(2012)073 [arXiv:1110.4601 [hep-th]].
- [122] M. Blake, S. Bolognesi, D. Tong and K. Wong, “Holographic Dual of the Lowest Landau Level,” *JHEP* **12**, 039 (2012) doi:10.1007/JHEP12(2012)039 [arXiv:1208.5771 [hep-th]].
- [123] S. Kulkarni, B. H. Lee, J. H. Oh, C. Park and R. Roychowdhury, “Transports in non-conformal holographic fluids,” *JHEP* **03**, 149 (2013) doi:10.1007/JHEP03(2013)149 [arXiv:1211.5972 [hep-th]].
- [124] B. Swingle, L. Huijse and S. Sachdev, “Entanglement entropy of compressible holographic matter: loop corrections from bulk fermions,” *Phys. Rev. B* **90**, 045107 (2014) doi:10.1103/PhysRevB.90.045107 [arXiv:1308.3234 [hep-th]].
- [125] M. Fujita, S. Harrison, A. Karch, R. Meyer and N. M. Paquette, “Towards a Holographic Bose-Hubbard Model,” *JHEP* **04**, 068 (2015) doi:10.1007/JHEP04(2015)068 [arXiv:1411.7899 [hep-th]].
- [126] R. Argurio, J. Hartong, A. Marzolla and D. Naegels, “Symmetry breaking in holographic theories with Lifshitz scaling,” *JHEP* **02**, 053 (2018) doi:10.1007/JHEP02(2018)053 [arXiv:1709.08383 [hep-th]].
- [127] H. Wang, A. L. Chudnovskiy, A. Gorsky and A. Kamenev, “Sachdev-Ye-Kitaev superconductivity: Quantum Kuramoto and generalized Richardson models,” *Phys. Rev. Res.* **2**, no.3, 033025 (2020) doi:10.1103/PhysRevResearch.2.033025 [arXiv:2002.11757 [cond-mat.str-el]].
- [128] R. A. Costa-Silva and H. Boschi-Filho, “Anomalous and linear holographic hard wall models for glueballs and the pomeron,” *Phys. Rev. D* **109**, no.8, 086019 (2024) doi:10.1103/PhysRevD.109.086019 [arXiv:2306.04728 [hep-ph]].
- [129] R. A. Costa-Silva and H. Boschi-Filho, *Phys. Rev. D* **110**, no.8, 086014 (2024) doi:10.1103/PhysRevD.110.086014 [arXiv:2405.18599 [hep-ph]].
- [130] R. L. Workman *et al.* [Particle Data Group], “Review of Particle Physics,” *PTEP* **2022**, 083C01 (2022) doi:10.1093/ptep/ptac097
- [131] S. S. Gubser, I. R. Klebanov and A. M. Polyakov, “A Semiclassical limit of the gauge / string correspondence,” *Nucl. Phys. B* **636**, 99-114 (2002) doi:10.1016/S0550-3213(02)00373-

- 5 [arXiv:hep-th/0204051 [hep-th]].
- [132] M. Henningson and K. Sfetsos, Phys. Lett. B **431**, 63-68 (1998) doi:10.1016/S0370-2693(98)00559-0 [arXiv:hep-th/9803251 [hep-th]].
- [133] W. Mueck and K. S. Viswanathan, “Conformal field theory correlators from classical field theory on anti-de Sitter space. 2. Vector and spinor fields,” Phys. Rev. D **58**, 106006 (1998) doi:10.1103/PhysRevD.58.106006 [arXiv:hep-th/9805145 [hep-th]].
- [134] W. Rarita and J. Schwinger, “On a theory of particles with half integral spin,” Phys. Rev. **60**, 61 (1941) doi:10.1103/PhysRev.60.61
- [135] A. Volovich, “Rarita-Schwinger field in the AdS / CFT correspondence,” JHEP **09**, 022 (1998) doi:10.1088/1126-6708/1998/09/022 [arXiv:hep-th/9809009 [hep-th]].
- [136] E. Klempt and B. C. Metsch, “Multiplet classification of light-quark baryons,” Eur. Phys. J. A **48**, 127 (2012) doi:10.1140/epja/i2012-12127-1
- [137] E. Klempt and J. M. Richard, “Baryon spectroscopy,” Rev. Mod. Phys. **82**, 1095-1153 (2010) doi:10.1103/RevModPhys.82.1095 [arXiv:0901.2055 [hep-ph]].